Pathological and Functional Analysis of Combined Mutations Associated with Alzheimer's Disease in Mice

アルツハイマー病の複合変異が生体にもたらす病理学的および機能的影響の解析

Kaori SATO

佐藤　香織

February, 2022

Pathological and Functional Analysis of Combined Mutations Associated with Alzheimer's Disease in Mice

アルツハイマー病の複合変異が生体にもたらす病理学的および機能的影響の解析

Waseda University

Graduate School of Advanced Science and Engineering

Department of Life Science and Medical Bioscience

Research on Molecular Brain Science

Kaori SATO

佐藤　香織

February, 2022

Table of Contents

Abstract

Tremendous achievements for understanding pathophysiology of Alzheimer's disease (AD) have been made in transgenic mouse models that overexpress mutant disease-causal genes such as amyloid precursor protein (*APP*) and/or presenilin1 (*PSEN1*). However, such mouse models suffer from experimental limitations caused by overproduction of APP fragments such as C-terminal fragment β (CTF-β) that do not appear to accumulate in AD patients. We previously developed single *App* knock-in (KI) mouse models of AD, harboring the Swedish and Beyreuther/Iberian mutations with or without the Arctic mutation ($App^{NL\text{-}G\text{-}F}$ and $App^{NL\text{-}F}$ mice), not depending on APP overexpression. These models showed amyloid β peptide (Aβ) pathology, neuroinflammation and cognitive impairment in an age-dependent manner. The former line exhibits extensive pathology as early as 6 months but is unsuitable for investigating Aβ metabolism and clearance because the Arctic mutation renders Aβ resistant to proteolytic degradation and prone to aggregation. The weakness of the latter model is that it may take as long as 18 months for the pathology to become prominent. In addition, these models are inappropriate for use in preclinical studies of β-secretase inhibitors because the Swedish mutation influences the mode of β-secretase inhibitor action *in vivo*. To address these drawbacks, in this study, we have thus generated two additional lines of *App* knock-in mice. One exhibits early

deposition of wild-type human Aβ by crossbreeding the App^{NL-F} line with the $Psen1^{P117L/WT}$ line (*App*×*Psen1* double-mutant mice). I show that the effects of the pathogenic mutations in the *App* and *Psen1* genes are additive or synergistic. The other line devoid of the Swedish mutations (App^{G-F} mice) reveals that Verubecestat, a β-secretase inhibitor, inhibits Aβ production in App^{G-F} mice, but not in App^{NL-G-F} mice. The App^{G-F} mice started exhibiting Aβ pathology between 6 and 8 months of age, accompanying activation of microglia and astrocytes. I also found that the quantity of CTF-β failed to correlate with endosomal abnormality, implying that CTF-β may not be associated with endosome dysfunction observed in AD brains. These new AD mouse models provide new insights into understanding the etiology of AD and will help accelerate the development of disease-modifying therapies to treat preclinical AD.

Chapter 1. Introduction

1.1 Alzheimer's Disease

In 1906, a German psychiatrist, Alois Alzheimer reported for the first time a 51-year-old female patient with pronounced cognitive impairment, behavioral abnormality, hallucinations, delusions and psychosocial inability. The patient died four and a half years after the onset. At autopsy, he discovered "a tangle of fibrils" inside of cells and "the deposition of a special substance" in the cortex [51(4):9-111]. Although he originally named the disease presenile dementia, it has come to be known as the most prevalent cause of dementia, now referred to as Alzheimer's disease (AD) [2]. The population with dementia has reached 50 million worldwide, and about two thirds of them suffer from AD (World Alzheimer Report 2018). As Dr. Alzheimer described, the postmortem brain studies have pathologically shown that two primary hallmarks of senile plaques (SPs) and neurofibrillary tangles (NFTs) are inevitably associated with AD [3-5]. SPs are extracellular aggregates composed primarily of 38-49 amino acid residues termed amyloid beta peptides (Aβ), while NTFs are intracellular accumulations of hyper-phosphorylated form of tau protein which is required to the microtubule stability [6]. AD brains exhibit overaccumulation of SPs and NFTs followed by memory loss, progressive cognitive decline and severe atrophy (**Fig. 1a**). A symptomatic period prior to the onset

is named mild cognitive impairment (MCI), which is thought to be a reversible stage to prevent AD onset [7].

AD has been intensively investigated worldwide for over 100 years since firstly reported. There had been, however, no effective disease-modifying treatments available for AD until 2020. Dozens of studies targeting Aβ have been conducted as a therapeutic target by the research community, because excessive Aβ initiates to deposit more than 20 years before cognitive dysfunction clinically appears [8] (**Fig. 1b**). In fact, there is still controversy over the specific relationship between Aβ deposition and onset or progression of AD. One clinical trial of the anti-Aβ immunotherapy (AN-1792) might give an answer to this question. The trial targeting the subjects with probable AD uncovered that the treatment successfully and drastically excluded Aβ from brains, but it was not capable of either retrieving or stopping their cognitive decline [9]. There arises one possibility that, although Aβ deposits perform as a provoking lesion for AD pathogenesis toward neuronal degeneration, its removal does never attenuate the disease progression once the cognitive dysfunction appears. Other multiple immunotherapies also failed in clinical trials even though the treatments took robust effect on Aβ reduction in mice. Moreover, it is reported that efficacy of anti-amyloid immunotherapy depends on Aβ species or accumulating forms of Aβ deposited in brains [10], which thus drive confusing results with ease in

clinical and preclinical studies. Taken together, we have to take medicinal measures to conquer AD at the stage of just the kickoff of Aβ excess accumulation, and to utilize appropriate animal models for the efficient development of the next medications, especially considering anti-Aβ immunotherapy as a recent hot topic worldwide.

Surprisingly, breaking news came in on June 7, 2021. Aducanumab [11], one of the anti-Aβ human monoclonal antibodies obtained an approval from the U.S. Food and Drug Administration, even though a phase IV trial that will take at least ten years are strictly required. More than 15 years passed since the latest drug was approved as a medication to beat against AD, which thus gave us some hope. However, the treatment with aducanumab requires the intravenous drip once every four weeks, costs approximately 56,000 dollars a year and gives only a modest profit for patients [12]. Although only 4 drugs other than aducanumab have been prescribed for patients now, they have no obvious effect on disease progression and have potential side effects commonly including nausea, diarrhea, insomnia, vomiting, constipation, headache, loss of appetite, bowel movements, confusion and dizziness in many cases, thus being hard to use continuously [13-16]. We long for any drugs that have truly cost- and health- beneficial effects on patients, their families and our society.

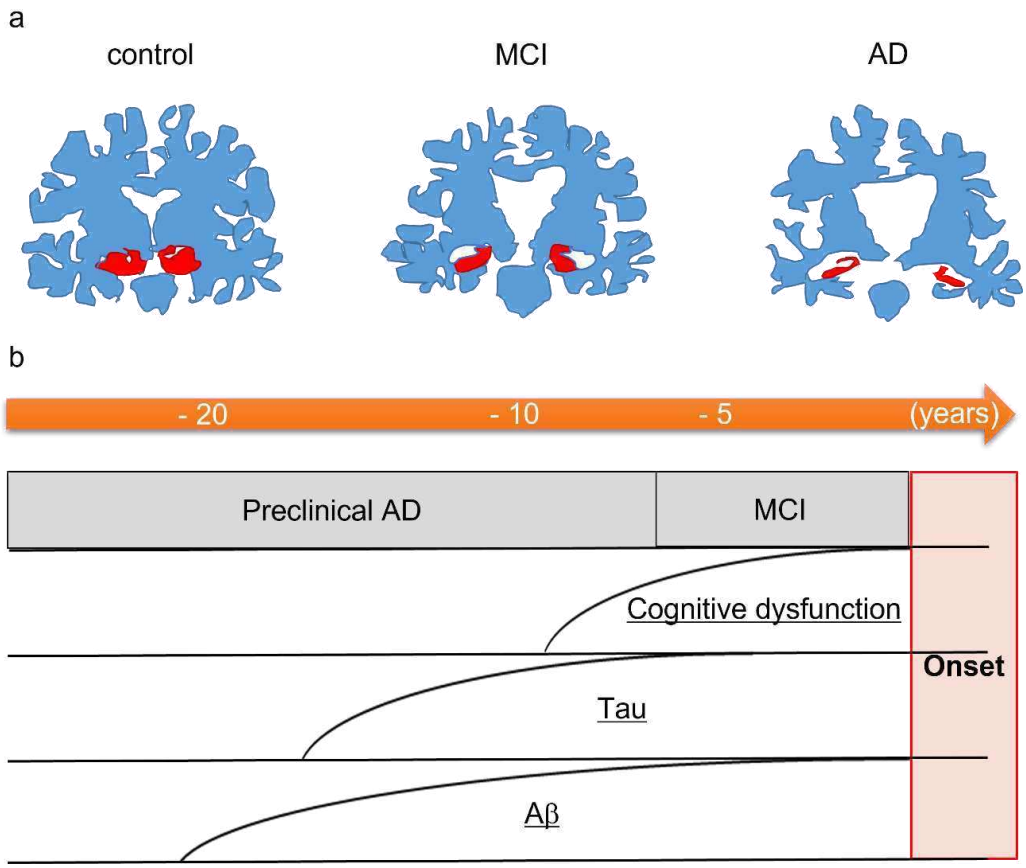

Fig. 1. An overview of the AD progression. **a** Schematic images indicate the extent of brain atrophy (blue) at healthy, MCI and AD stages. Severe hippocampus (red) atrophy and ventricular enlargement observed in AD patients [17]. **b** A time series of the disease progression from preclinical period to the onset.

1.2 Amyloid Precursor Protein

Amyloid Precursor Protein (APP), one of the single-pass transmembrane proteins, belongs to the highly conserved APP-related family including APP and amyloid precursor-like protein in mammals, amyloid precursor-like 1 in *C. elegans* and amyloid precursor protein-like in *Drosophila*. All of these have large N-terminal domains in lumen as well as a short cytoplasmic C-terminal domain. Aβ peptides are produced from only APP through two secretases-mediated sequential processing, not from amyloid precursor-like protein in *C. elegans* and Drosophila [18]. APP is initially truncated through physiological processing pathways either by α-secretase within Aβ sequence, by β-secretase at the amino terminal end of Aβ, or by η-secretase outside Aβ region in the extracellular domain. These processes produce three large ectodomains and C-terminal residues: a soluble N-terminal fragment α (sAPPα) and C-terminal fragment α (CTF-α), sAPPβ and CTF-β, or sAPPη and CTF-η, respectively (**Fig. 2a**). CTF-α and CTF-β are subjected to the subsequent cleavages by γ-secretase, leading to the production of p3 fragment, Aβ and the APP intracellular domain (AICD) in both pathways. CTF-η undergoes following proteolysis by α-secretase and β-secretase, which results in the formation of Aη peptides termed Aη-α and Aη-β. CTF-η is further rifted by γ-secretase to produce AICD [19].

What is the physiological function of APP? Some groups have reported that the normal roles of APP using APP knock-out (KO) mice. APP-KO mice that are viable and fertile exhibited 15-20% reduction of the body weight, phenotypic abnormality in neuronal or muscular activity and deficits in long-term potentiation and retention of memory [20, 21]. APP is increased in response to hypoxic conditions and the risk of mortality against cerebral ischemia was greatly increased in APP-KO mice [22]. sAPPα displays protective roles against dendritic spine loss induced by Aβ oligomer accumulation [23]. On the other hand, sAPPβ is identified as a ligand for Death Receptor 6, a member of the tumor necrosis factor receptor that induces the activation of caspase 3 and 6, leading to neurodegeneration [24]. These results suggest that APP itself is not such as to serve as a crucial protein for a matter of life or death during embryonic development but plays important roles in neurogenesis, synaptic transmission, learning and memory, neurodegeneration and other toxic conditions.

How are Aβ species produced following secretase-mediated pathways? CTF-β are further subjected to the consecutive trimmings by γ-secretase so that a variety of Aβ species in different lengths including 38-49 amino acid compositions which depends on the cleavage site by γ-secretase. Cell-based experiments suggest that Aβ truncating process includes the following two lines: Aβ49→Aβ46→Aβ43→Aβ40 and Aβ48→

Aβ45→Aβ42→Aβ38 [25, 26] (**Fig. 2b**). Aβ40 is the most common in our nature, while longer forms of Aβ such as Aβ42 or Aβ43 exhibits more hydrophobic, neurotoxic and fibrillogenic characters which are prone to aggregate in the brain [27]. Increase in Aβ42 and Aβ43 or Aβ42/Aβ40 ratio are associated with pathological environment which causes AD onset. In this way, enzymatic secretion of Aβ involving in β-secretase is believed to be the amyloidogenic line, while the non-Aβ producing processing in which α-secretases participate is often called non-amyloidogenic pathway [28].

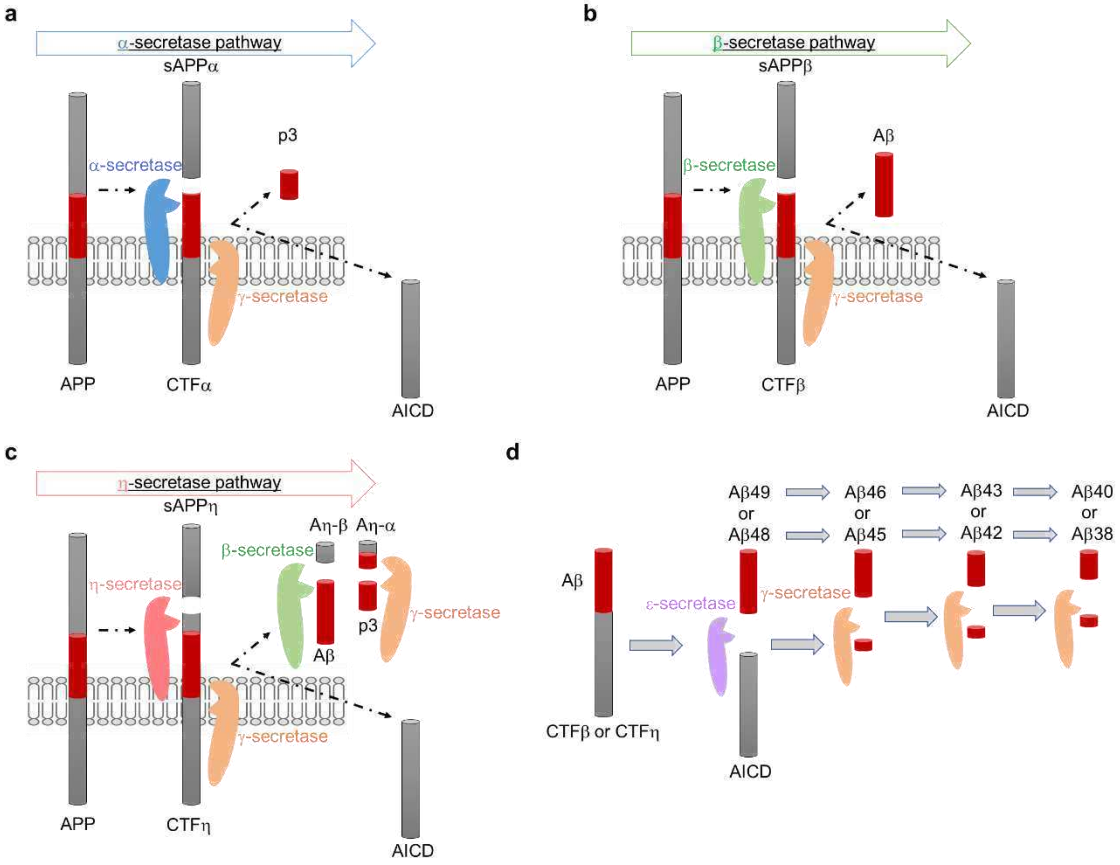

Fig. 2 APP processing via specific secretases-mediated sequential cleavages. **a-c** Three major pathways related to APP processing. **d** APP CTFs are processed to generate different length of Aβ species. Secretases indicated in color are shown as follows; α- (blue), β- (green), γ- (orange), η- (pink) and ε- (purple) secretases.

1.3 Presenilin

Presenilin (*PSEN*, PS) is a protein that holds 9 transmembrane domains. *PSEN1* on chromosome 14 and *PSEN2* on chromosome 1 encode PS1 and PS2, respectively. PS1 and PS2 share similar structures and functions with 67% identity to each other [29]. PS functions as catalytic subunits of the γ-secretase directly cleaving APP and other type 1 transmembrane proteins including Notch which is critically involved in cell differentiation and embryogenesis [30]. PS is firstly synthesized as a 50kDa protein, followed by cleavage via autolysis processing into two fragments to form active γ-secretase [31]. Some genetic mutations located at the cleavage stie result in a dominant-negative form of γ-secretase [32]. Not just PS but also other components, which help mature two cleaved fragments of PS, are required for γ-secretase to display functional activity [33]. PS1-deficient mice die shortly after birth with varying degrees of hemorrhages or deformative ribcages [34]. PS1 conditional knock-out mice is viable and apparently normal but show deficits in synaptic plasticity [35] PS1 is eliminated in neocortex and hippocampus in this line. In PS1 and PS2 conditional double knock-out mice, severe inflammation spread in brain and in periphery with enhanced oxidative damage [36, 37]. This mouse line show inactivation of both PS1 and PS2 in excitatory neurons in the forebrain cortex. These abnormalities are caused by malfunction of γ-

secretase that cleaves a bunch of substrates in mammals. Although PS1 deficiency has been well studied before, it remains unclear that pathogenic or other mutations in the *PSEN1* gene lead to functional consequences in living animals.

1.4 Genetic variants associated with AD

AD can be divided into two types: late-onset sporadic AD (LOAD) and early-onset familial AD (EOAD). LOAD, defined as its onset after 65 years of age, accounts for more than 95% of all AD cases. EOAD, beginning by the age of 60, is the rest of cases [38]. As sequencing technologies have made rapid advances, over 400 disease-associated genetic variants (Alzforum, http://www.alzforum.org) have been identified as disease-associated mutations in the *APP* and *PSEN* genes where EOAD, inherited forms of the disease, carry mutations in many cases. These genes are primarily involved in the process of Aβ production [39, 40]. In particular, *PSEN1* is the most frequent causal gene, in which over 300 mutations have been reported (**Fig. 3**). Some pathogenic mutations, for instance, drastically elevate total Aβ production with the β-secretase processing activated. Others can increase Aβ42 secretion thereby contributing to change in Aβ42/Aβ40 [41, 42], which leads to early onset of AD.

However, it remains elusive that each genetic variants result in any functional consequences, especially *in vivo*. To this end, Sasaguri et al. generated multiple lines of mutant mice harboring point mutations and suggested the possibility that a number of genetic variants exist whose physiological effects are not still uncovered [41]. In 2012, Icelandic mutation (A673T) was identified in the *APP* gene as the first protective

mutation that results in 40% reduction of total Aβ production, and more interestingly, A673T even defends against cognitive decline in the healthy elderly [43-45]. A few decades ago, some researchers indicated that Aβ quantity in the brain strongly linked to dementia associated with AD [46], but there has been no firm evidence for a long time. The striking discovery of A673T mutation supports the hypothesis that Aβ acts as a causal molecule in AD pathogenesis. Nagata et al. demonstrated using AD mouse models that a 34 bp deletion mutation in 3'UTR results in a substantial reduction of Aβ deposition *in vivo* [47], indicating that there exists less-frequent but promising variants protective or pathological against AD which have not seen the light of the day in human.

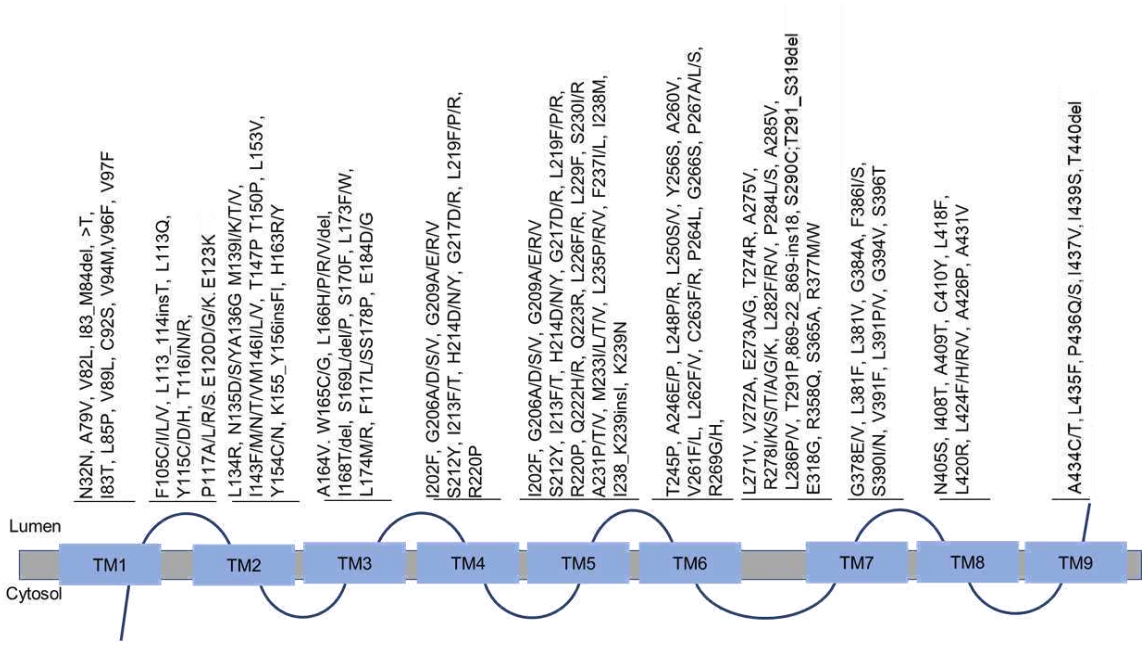

Fig. 3 Pathogenic mutations in the *PSEN1* gene. P117L mutation is introduced into endogenous mouse *Psen1* in this study. More than 300 mutations including whose pathogenicity remain unknown are reported as of September 2021 described in Alzforum (https://www.alzforum.org/mutations/psen-1).

1.5 Mouse models in AD research

To date, no clear explanation can address what increases the LOAD risk without any mutations although EOAD cases are mostly caused by pathogenic mutations in the *APP* or *PSEN* genes. However, the two distinct hallmarks, Aβ deposition and tau aggregates in the brain, commonly underly both sporadic and familial types of AD, which allows us to apply mutant animal models to understand pathophysiology of both EOAD and LOAD. Making the most use of functional consequences of pathogenic mutations, over 180 genetically modified mouse models containing AD-linked mutations have been generated, and in many instances these mice have yielded significant insights into underlying pathogenic mechanisms. For the past two decades, transgenic (Tg) mice overexpressing mutant *APP* and/or *PSEN1* cDNA(s) have been globally used as AD mouse models [48]. In this manuscript, "transgenic" means that foreign genes are inserted into unknown loci with multiple copies, in most cases. Tg mice exhibit not just excessive Aβ plaque burden in the brain but also behavioral abnormality and sometimes neuronal cell loss. Such mouse models, however, often suffer from experimental limitations caused by overproduction of APP fragments such as CTFs and AICD, both of which do not appear to accumulate in AD brains and may induce artificial endosomal abnormalities [49] and transcriptional malfunctions [50], respectively. Other overexpression artifacts include

calpain activation [51], calpastatin deficiency-induced early lethality [52], endoplasmic reticulum stresses [53] and sudden death with lethal epilepsy. In addition, Gamache *et al.* demonstrated that the random insertion of transgene(s) destroyed unexpectedly large regions in endogenous gene loci of the host animal [54]. It is highly recommended that all Tg models overexpressing *APP* or *APP*/*PSEN1* that are being used in research should be subjected to whole genome sequencing to identify the destroyed loci that may affect their phenotypes.

To overcome these drawbacks, we previously generated $App^{NL\text{-}G\text{-}F/NLG\text{-}F}$ knock-in (KI) ($App^{NL\text{-}G\text{-}F}$) and $App^{NL\text{-}F/NL\text{-}F}$ -KI ($App^{NL\text{-}F}$) mice that contain humanized sequences in the murine Aβ sequence, and also harbor the Swedish (KM670/671NL) [55] and Beyreuther/Iberian (I716F) [56] mutations with or without the Arctic (E693G) [57] mutation [48, 58]. These mice showed typical Aβ pathology, neuroinflammation and memory impairment and are being used by more than 500 research groups world-wide. The Aβ pathology is quite similar to that observed in human, which means that Aβ42, not Aβ40, is predominantly accumulated earlier in the brain [58], [59]. Moreover, abnormal behavior appears after Aβ deposition initiates, while some Tg mice exhibit cognitive deficits preceding the amyloid pathology, which is not consistent with the human pathology. In this way, *App*-KI mice were generated using knock-in strategy, not gene

overexpression, opened a new era in the AD research community. KI technology have enabled us to generate animal disease models that recapitulate human pathology, or to elucidate the functional consequences of the pathological mutations *in vivo*. Although it takes a lot of time and money to precisely induce knock-in mutations until several years ago, it will become much easier as the genome editing technology rapidly progresses.

1.6 Genome engineering technology

With the rapid development of the gene sequencing technology, the number of genetic variants has been increasing, whether they are pathogenic or not. In order to determine whether mutations are truly linked to the pathogenesis of diseases, genome engineering strategies greatly helps us introduce intended mutations into any loci *in vitro* and *in vivo*. Programmable genome editing tools include zinc-finger nucleases (ZFN) and transcription activator-like effector nucleases (TALEN) [60, 61]. ZFN and TALEN are engineered chimeric proteins composed of sequence-specific DNA binding modules fused to a nuclease catalytic domain, which can induce double-strand breaks (DSB) [60]. TALEN firstly reported in 2010 took the place of ZFN that has limitations such as interference between multiple modules to recognize DNA and difficulty in making process of robustly functional protein arrays. In 2013, however, clustered regulatory interspaced short palindromic repeats/CRISPR-associated proteins (CRISPR/Cas) has newly emerged as a highly evolved tool for genome modification [62, 63]. The CRISPR/Cas system has greater advantages over the previous two techniques and has spread rapidly all over the world. <1]>The targeted sequence is recognized by RNA-DNA complementary binding, different from the protein-DNA specific binding for ZFN and TALEN. <2> DSB requires a single-guide RNA (sgRNA) and a single endonuclease

termed Cas protein, while a pair of chimeric proteins for ZFN and TALEN. <3> Researchers can prepare genome editing tools in their labs more easily than ZFN and TALEN. <4> The efficiency and easiness enable us to target multiple sites simultaneously. In these respects, nothing compares to the CRISPR/Cas technology for its usefulness and higher efficiency.

There is still, however, room for improvement. sgRNA binds to the opposite strand of target sequence with the recognition of protospacer adjacent motifs (PAM) associated with Cas proteins. The PAM sequence strictly narrowed the number of targetable sites in genome. To broaden applications of CRISPR/Cas system for genome editing, various Cas proteins recognizing different PAMs have been discovered from specific bacteria. A Cas9 protein derived from *Straphylococcus aureus* (SaCas9) that recognizes 5'-NNGRRT-3' was identified [64, 65], for instance, while SpCas9 from *Streptococcus pyogenes* that recognizes 5'-NGG-3' has been the most frequently used in the world. Genome editing using SaCas9 would exhibit higher specificity and fewer off-target effects compared to using SpCas9. Moreover, many researchers have developed mutagenized Cas9 proteins that recognize alternative PAM sequences via directed evolution methods *in vitro* [66, 67].

DSB can be successfully remediated following donor templates via homologous directed repair (HDR) pathway but frequently repaired with small and large insertion or

deletion (indel) mutations through nonhomologous end joining (NHEJ) (**Fig. 4a**). Cas9 proteins efficiently induce DSB at target sites, but they can also easily evoke additional cleavages into non-target genomic regions including a few mismatches. Indel formation is unwanted especially for introduction of single nucleotide polymorphism or mutations.

To this end, a precise and efficient DNA base editing (BE) system was firstly unleashed to the world [68]. BE enables us to introduce a single base substitution without any cleavage and repair template, whereas using a conventional CRISPR/Cas system a donor template is necessary to induce a targeted knock-in mutation. Cytosine base editor is a catalytically inactivated Cas9 (nCas9) fused to a rat cytidine deaminase (APOBEC1) and uracil glycosylase inhibitor (UGI) [69]. APOBEC1 deaminates cytosine to uracil, leading to a UG base pair, subsequent UA combination and remediation to a TA pair through endogenous repair mechanisms, thus resulting in C to T substitutions (**Fig. 4b**). UGI can act as an inhibitor against the cellular repair pathway that removes deaminated bases and change into WT. The editing window of CBE is open for 4-8 positions, counting the distal end of the PAM as position 1 [68]. BE system reduces number of off-target effects compared to the conventional CRISPR/Cas, as the editing can achieve a single base substitution without DSBs. Altogether, the CRISPR/Cas and BE technologies efficiently introduce not just knock-in or knock-out modification but also a point mutation

to generate mutant animal models harboring disease-associated genetic variants.

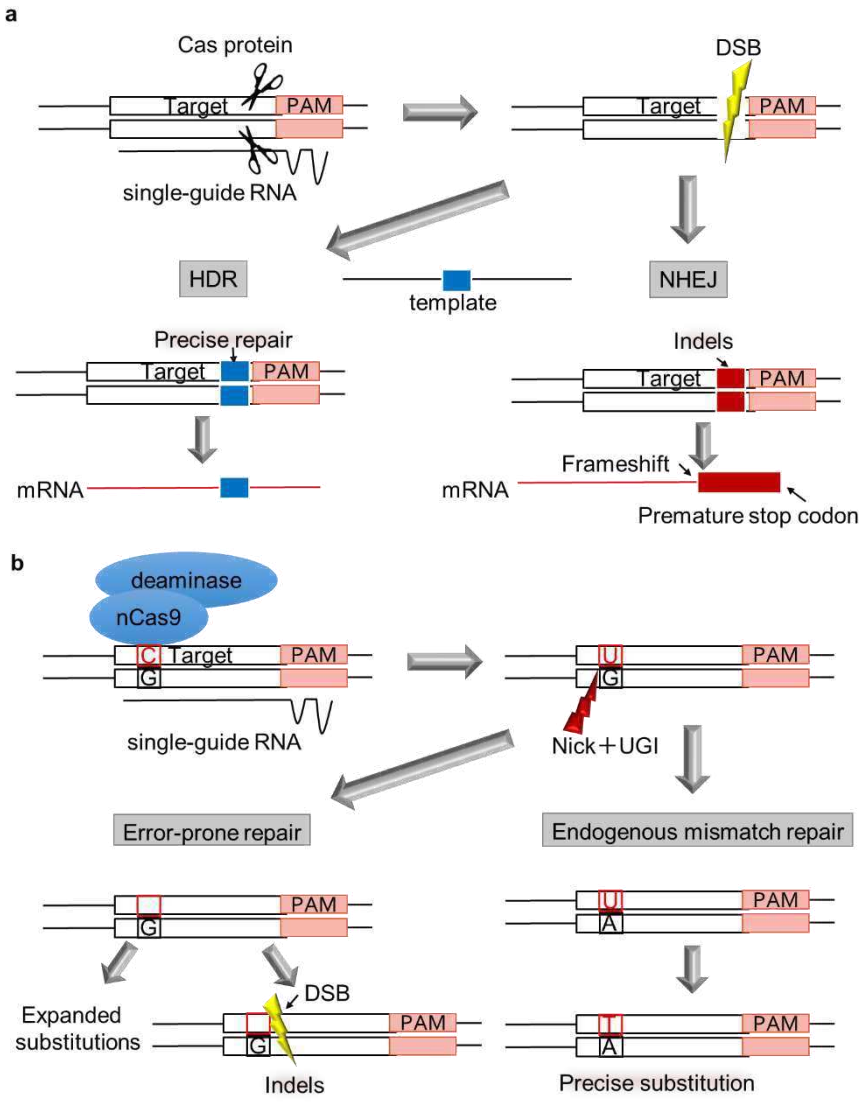

Fig.4 Schematic images of genome modification pathway. **a** DNA repair following CRISPR/Cas-mediated DSB. **b** Base editing system can induce a single base substitution without DSB, reducing indel mutations compared to the conventional CRISPR/Cas system.

1.7 Endosomal trafficking

Endocytosis is one of the fundamental systems for cell survival. Extracellular substances are subjected to endocytosis and transported to degrading or synthetic pathways. All transport vesicles firstly arrive at early endosome that plays crucial roles in endocytic sorting system. In AD, early endosome enlargement is observed as an early cytopathological manifest preceding amyloid burden, tau accumulation and cognitive impairment [70, 71]. A recent genome wide association study identified AD risk genes including multiple genes related to endosomal function [72]. These pathological and genetic lines of evidence indicate endosomal abnormality might be a pathological sign leading to the onset of both early- and late-onset AD. Several *in vitro* studies suggest that the quantity of CTF-β contributes to induce early endosome enlargement, which is independent of Aβ deposition [49], [73] and that APP itself exists in the enlarged early endosomes. However, it still remains unclear that CTF-β or Aβ affect the early-endosomal dysfunction *in vivo*.

Chapter 2. Materials and Methods

Animals

All animal experiments were conducted in compliance with regulations stipulated by the RIKEN Center for Brain Science. App^{NL-F} and App^{NL-G-F} mice bearing two and three familial AD mutations, respectively [Swedish (KM670/671NL) and Beyreuther/Iberian (I716F) with or without the Arctic (E693G) mutation], driven by the endogenous promoter, as well as the humanized Aβ sequence, were generated described previously[58]. $Psen1^{P117L}$ mice [41] were crossed with the App^{NL-F} mice to generate *App*/*Psen1* double mutant mice. All double mutant mice used were homozygous for the *App* mutations and heterozygous for the *Psen1* mutation ($App^{NL-F}Psen1^{P117L}$). In the $App^{NL-F}Psen1^{P117L}$ study, male mice were used for biochemical analyses and both male and female mice were used for immunohistochemical studies. App^{NL-G-F} and ICR mice were used as zygote donors and foster mothers, respctively. C57BL/6J and App^{NL} mice were prepared as controls [58]. All mutant mice used in the App^{G-F} study were homozygous for the expressed mutations. Both male and female mice were used in the App^{G-F} experiments. All mice were bred and maintained in accordance with regulations for animal experiments promulgated by the RIKEN Center for Brain Science.

Generation of *Psen1*^{P117L} mice

sgRNAs were designed using in silico tools including sgRNA designer (https://crispr.med.harvard.edu/) and Cas/OFFinder (http://www.rgenome.net/cas-offinder/). sgRNA targeted the ACCCCATTCACAGAAGACAC sequence in exon 5 in the *Psen1* gene. VQR-BE that recognizes NGA as the PAM sequence was used for the genome editing. VQR-BE mRNA were transcribed *in vitro* using pBK-VQR-BE3 (#85171, Addgene) using mMESSAGE mMASHINE T7 Ultra Transcription Kit (AM1345, Thermo Fisher Scientific). For BE mRNA synthesis, the transcript template was generated via PCR using Herculase 2 Fusion DNA polymerase (#600675, Agilent Technologies) with the specific primers with T7 promoter as listed in **Table 1**. For sgRNA synthesis, the sgRNA template were prepared through PCR using the MEGAshortscript T7 Transcription Kit (AM1354, Thermo Fisher Scientific). PCR products were purified using QIAquick PCR Purification Kit (#28106, QIAGEN). Synthesized mRNA and sgRNA were purified using the MEGAclear Transcription Clean-Up Kit (AM1908, Thermo Fisher Scientific). Prepared sgRNA (30 ng/μl) and mRNA (200 ng/μ) were injected into the cytoplasm of mouse zygotes. The founder mice carrying P117L mutation were generated with high efficiency (46.3%) and backcrossed with wild-type C57BL/6J to obtain F1 mice[41]. I confirmed the homozygotes were alive and fertile.

sgRNA	
T7-P117	TAATACGACTCACTATAGGACCCCATTCACAGAAGACACGTTTT AGTACTCTGG
Tail primer	AAAAATCTCGCCAACAAGTTGACGAGATAAACACGGCATTTTG CCTTGTTTTAGTAGATTCTGTTTCCAGAGTACTAAAAC
SaCas9 mRNA	
T7-BE-F	GCCGCTAATACGACTCACTATAG
T7-BE-R	GCGGGTTTAAACTCAATGGT

Table 1. Information on primers and oligonucleotides used for the synthesis of sgRNA and VQR-BE mRNA.

In vitro synthesis of CRISPR tools was performed with the listed primers for the generation of *Psen1*^{P117L} mice. See Methods for details.

Generation of *App*$^{G\text{-}F}$ mice

sgRNA targeting mouse *App* exon 16 was designed utilizing the CRISPR design tool [74]. To reduce the possibility of off-target events, SaCas9 that recognizes NNGRRT as the PAM site was selected to introduce double-stranded breaks. ssODN was designed to cause NL670/671KM substitution (AATCTA>AAGATG) overlapping the PAM region so that the oligonucleotide did not include silent mutations, thus preventing re-binding and recutting after the desired genome modification via homology-directed repair. pX601 plasmid (Addgene, #61591) was used for *in vitro* transcription of SaCas9 mRNA, and sgRNA was synthesized as described previously [75]. Information of the primers and oligonucleotides used for the *in vitro* synthesis of CRISPR tools is listed in **Table 2**. The prepared SaCas9 mRNA (100 ng/μl) and sgRNA (100 ng/μl) along with ssODN (100 ng/μl) were co-injected into the cytoplasm of the heterozygous *App*$^{NL\text{-}G\text{-}F}$ mouse zygotes. Founder mice were identified by PCR and sequencing analysis of the target site and crossed with wild-type mice to obtain heterozygous F1 mice.

sgRNA	
T7_sgRNA_moAPP_NL_KM_F	TGTAATACGACTCACTATAGGAAGACGGAAGAGATCTCGGAAGTTTTAGTACTCTGGAAACAGAATC
sgRNA_SaCas9_tail_R	AAAAATCTCGCCAACAAGTTGACGAGATAAACACGGCATTTTGCCTTGTTTTAGTAGATTCTGTTTCCAGAGTACTAAAAC
SaCas9 mRNA	
T7_SaCas9_F	TAATACGACTCACTATAGGGCCCCATTGACGCAAAT
T7_SaCas9_R	GGCAACTAGAAGGCACAGTCGA
ssODN	
APP_Ex16_NL_KM_ssODN	caatctcggggagaggcagtttatttttgcctacCAGTTTTTGATGGTGGACTTCATATCCTGAATCATGTCTGAATTCTGCATCCATCTTCACTTCCGAGATCTCTTCCGTCTTGATGTTTGTCAGCCCAGAACctgcgtcaaacacaaagtatgcagggccatccgttagtgtgaccgccagccacaaggaggcaaa

Table 2. Information on primers and oligonucleotides used for the synthesis of sgRNA, SaCas9 mRNA and ssODN.

In vitro synthesis of CRISPR tools was performed with the listed primers for the generation of $App^{G\text{-}F}$ and $App^{huA\beta}$ mice. See Methods for details.

Generation of *App*$^{huA\beta}$ mice

To generate *App*$^{huA\beta}$ mice that carried only the humanized Aβ sequence, virtually the same strategy was used to that employed for developing *App*$^{G\text{-}F}$ mice. The prepared sgRNA, mRNA and ssODN were identical to those used for *App*$^{G\text{-}F}$ mice, with the only difference being that *App*^{NL} zygotes instead of *App*$^{NL\text{-}G\text{-}F}$ zygotes were used for injecting genome editing tools. Potential off-target sites were also identical as those for *App*$^{G\text{-}F}$ mice.

Off-target effect analysis

Candidate sequences were identified *in silico* using COSMID (https://crispr.bme.gatech.edu/) [76] and Cas-OFFinder (http://www.rgenome.net/cas-offinder/) [77] allowing up to 3 bp mismatches and 1 bp DNA and/or RNA bulge. Genomic DNA extracted from mouse tails was amplified by PCR with the primers listed in **Table 3**. All genomic sequences of the amplicons were analyzed by Sanger sequencing using a DNA sequencer (ABI 3730xl).

Genotyping

Genomic DNA was extracted from mouse tails in lysis buffer (10 mM pH 8.5 Tris-HCl,

5 mM pH 8.0 EDTA, 0.2% SDS, 200 mM NaCl, 20 μg/ml proteinase K) followed by concentrating and desalting with ethanol. Purified DNA was subjected to PCR and followed by Sanger sequencing analysis with the specific primers according to a previous report employing *App*-KI mice, including App^{NL}, App^{NL-F} and APP^{NL-G-F} strains [58]. Genotyping primers for $App^{NL-F}Psen1^{P117L}$ mice have been described previously [41, 58] and for App^{G-F} mice are listed in **Table 3**.

Genotyping of *Psen1*^{P117L}mice	
PS1_gDNA_Ex5_F	GGTTGACTGATGACCTGCAA
PS1_gDNA_Ex5_R	GCTCAGAACGTGACGCTTAC
Genotyping of *App*$^{G\text{-}F}$ and *App*$^{huA\beta}$ mice	
moAPP_Ex16_hs_F2	ACAGGCATTACATATTCAGCGT
moAPP_Ex16_hs_R2	ACTATCAACAGAGCCCCACT
Off-target analysis	
OFF1_F	CCATGCATTGTCTTTGAACCT
OFF1_R	CGCCTCTGAATTCCTTGAA
OFF2_F	CAGGCTGTGGGATAGGTTTT
OFF2_R	CGAGGTCAGCTTGGCTTTTA
OFF3_F	CTGAAGAAGAGCCAGCCTCA
OFF3_R	TCTCAGGGAATCCACCATTC
OFF4_F	AGTAACAGCCCAGGCAGAAA
OFF4_R	TGCTAAGACACATAAAAACAAGCA
OFF5_F	GGACCCGAGTTTGATTCTCA
OFF5_R	CCTGTTTCTTCGGCATGTTT
OFF6_F	TTCTCCTTTCAGAAGATGTTTGG
OFF6_R	TTTCAATGTTCACCCCATCC
OFF7_F	ACGGAAGATTCCAGCTCAGA
OFF7_R	CCAGCACTCAATGCATGTTC
OFF8_F	GAGACGCTTTTGGACTTGCT
OFF8_R	TTTGCCAGCTGCAGATAATTT
OFF9_F	TCCTAGAGGAGTTTGGGGATT
OFF9_R	AGCTACAGGGCATCAAAAGC
OFF10_F	GGCCAATGCAGGTAGAATGT
OFF10_R	GCCTTTTCATATTGCCCTCA

Table 3. List of primers used for genotyping and off-target analyses.

All primer pairs were used for PCR and subsequence sequencing analyses. The sequential number of OFF primers corresponds to that of the potential off-target sites shown in

Figure 10. See Methods for details.

Brain sample preparation

Mice were anesthetized with isoflurane, transcardially perfused and fixed with 4% paraformaldehyde in PBS. The brains were dissected on ice into two halves at the midline. One hemisphere was divided into several parts and stored at -80℃ for biochemical analysis, while the other was incubated at 4℃ for 24 h and rinsed with PBS until paraffin processing for histochemical analysis.

Western blotting

Mouse brain tissues were homogenized in lysis buffer containing 50 mM Tris pH 7.6, 0.15 M NaCl, 1% Triton and cOmplete protease inhibitor cocktail (Roche Diagnostics) using a Multi-beads shocker (Yasui Kikai). Homogenates were incubated at 4℃ for 1 h and centrifuged at 15000 rpm for 30 min, and the supernatants were collected as loading samples. Concentrations of protein samples were measured with the aid of a BCA protein assay kit (Thermo Fisher Scientific). Equal amounts of proteins were subjected to sodium dodecyl sulfate-polyacrylamide gel electrophoresis (SDS-PAGE) and transferred to PVDF membranes (Invitrogen). For detection of APP-CTFs, delipidated samples were loaded onto membranes and boiled for 5 min in PBS before blocking with ECL

primeblocking buffer (GE Healthcare). After washing and blocking at room temperature, the membranes were incubated at 4℃ overnight with primary antibodies against APP, APP-CTFs, β-Actin or GAPDH as a loading control. Primary antibody dilution ratios are listed in **Table 4**. Targeted proteins were visualized with ECL select (GE Healthcare) and a Luminescent Image Analyzer LAS-3000 Mini (Fujifilm).

Immunostaining

Paraffin-embedded mouse brains were sectioned (thickness 4 μm) and subjected to deparaffinization processing; antigen retrieval was then performed by autoclaving at 121℃ for 5 min. Brain sections were treated with 0.3% H_2O_2 in methanol solution for 30 min to inactivate endogenous peroxidases. Sections were washed with TNT buffer (0.1 M Tris pH7.5, 0.15 M NaCl, 0.05% Tween20), blocked for 30 min using a TSA Biotin System kit (NEL703001KT, AKOYA BIOSCEIENCES) and incubated at 4℃ overnight with primary antibodies diluted in TNB buffer (0.1 M Tris pH 7.5, 0.15 M NaCl). Primary antibody dilution ratios are listed in **Table 5**. Primary antibodies against early endosome antigen 1 (EEA1) and α-smooth muscle actin is used to detect early endosome and cerebral amyloid angiopathy (CAA), respectively. Sections were rinsed, incubated with biotinylated secondary antibody and a tyramide signal amplification system used to detect

amyloid pathology as described previously [78]. For detection of glial activation, CAA and early endosome pathology, secondary antibodies conjugated with Alexa Fluor 488 or 555 diluted in 0.2% casein in PBS were used. Before mounting with PermaFluor (Thermo Fisher Scientific), sections were when necessary treated for 15 min with Hoechst33342 (Thermo Fisher Scientific) diluted in PBS. Photographic images were obtained using a confocal laser scanning microscope FV-1000 (Olympus), a NanoZoomer Digital Pathology C9600 (Hamamatsu Photonics) and EVOS M5000 Imaging System (Thermo Fisher Scientific). Quantification of immunoreactive signals was performed using Metamorph Imaging Software (Molecular Devices) and Definiens Tissue Studio (Definiens).

Antibody	Dilution ratio	#Manufacturer or reference
APP	1:10000	#MAB348, Millipore
APP-CTFs	1:1000	#A8717, Sigma-Aldrich
β-Actin	1:5000	#A5316, Sigma-Aldrich
GAPDH	1:150000	# 60004-1-Ig, Proteintech

Table 4. List of primary antibodies used for immunohistochemistry.

Primary antibody dilution ratios are shown. See Methods for details.

Antibody	Dilution ratio	#Manufacturer or reference
$A\beta_{40}$	1:100	#10047, IBL
$A\beta_{42}$	1:100	#18582, IBL
$A\beta_{43}$	1:50	#18583, IBL
$A\beta_{3(pE)\text{-}X}$	1:400	Saido et al., 1996[79]
N1D	1:200	Saido et al., 1996[80]
82E1	1:500	#10326, IBL
EEA1	1:100	#3288, Cell Signaling
α-smooth muscle actin	1:1000	#A2547, Sigma-Aldrich
Iba1	1:200	#013-27691, Wako
GFAP	1:200	#MAB3402, Millipore
PSD-95	1:50	#124011, Synaptic Systems
synaptophysin	1:200	#61012, PROGEN
Hoechst33342	1:5000	#H3570, Thermo Fisher Scientific

Table 5. List of primary antibodies used for immunohistochemistry.

Primary antibody dilution ratios are shown. See Methods for details.

DAB staining

Targeted signals were detected and visualized using VECTASTAIN *Elite* ABC Rabbit IgG kit (Funakoshi) and DAB・TRIS tablets (Mutokagaku). After deparaffinization and antigen retrieval treatment of mouse brain sections, endogenous peroxidases were inactivated using 0.3% H_2O_2 solution for 30 min. Sections were blocked with 3 drops of goat serum in 10 ml PBS for 30 min at room temperature and incubated with N1D antibody at 4℃ overnight. Sections were rinsed with PBS and incubated with the *Elite* ABC solution for 30 min and subsequently stained with DAB solution following the manufacturer's instructions. Before mounting, dehydration treatment was performed.

FSB staining

The PFA-fixed tissue sections were deparaffinized, incubated in 0.01% FSB solution in ethanol for 30 min and then rinsed in saturated Li_2O_3 in water for 15-20 sec at room temperature. The sections were differentiated in ethanol for 3 min followed by immersion in water for 5 min to stop the reaction. Readers should refer to the *Immunostaining* section concerning methods for subsequent treatments following antigen retrieval.

Enzyme-linked immunosorbent assay (ELISA)

Mouse brain samples were homogenized in a lysis buffer (50 mM Tris-HCl pH7.6, 150 mM NaCl and protease inhibitor cocktail) using a Multi-beads shocker (Yasui Kikai). The homogenates were centrifuged at 70000 rpm at 4℃ for 20 min, and the supernatant was collected as a Tris-Soluble (TS) fraction to which 1/11 vol of 6M guanidine-HCl (GuHCl) solution in 50 mM Tris and protease inhibitors were added. The pellet was loosened in lysis buffer with a Pellet Pestle (KIMBLE), dissolved in the 6M GuHCl buffer, and then sonicated at 25℃ for 1 min. The sample was incubated for 1 h at room temperature and then centrifuged at 70000 rpm for 20 min at 25℃ and the supernatant was collected as a GuHCl fraction. Tris-soluble and GuHCl-soluble fractions were loaded onto 96-well plates and incubated at 4℃ overnight using the Aβ ELISA kit (Wako) according to the manufacturer's instructions. For detection of Arctic Aβ produced from the brains of App^{NL-G-F} and App^{G-F} mice, standard curves were drawn using human Aβ peptides carrying the Arctic mutation as described previously [58].

Verubecestat administration

Verubecestat (ChemScene) dissolved in PBS was administrated orally to 3-month-old mice using a flexible sonde (FUCHIGAMI) at a single dose of 10 mg/kg according to Kennedy et al [81]. Three hours after a single treatment mouse brains were dissected and

stored at -80°C.

STATISTICAL ANALYSIS

All data are presented as the mean ± S.D. within each figure of the $App^{NL\text{-}F}Psen1^{P117L}$ study and shown as the mean ± S.E.M. within each figure of the $App^{G\text{-}F}$ study, respectively. For comparisons between two groups, data were analyzed by Student's *t*-test. For comparisons among more than three groups, I used one-way analysis of variance (ANOVA) followed by Tukey's multiple comparisons test. Two-way ANOVA followed by Sidak's multiple comparisons test was used when two data sets were analyzed. All statistical analyses were performed using GraphPad Prizm version 7.00 software (GraphPad software). Levels of statistical significance were presented as *P*-values: * $P < 0.05$, ** $P < 0.01$, *** $P < 0.001$.

Chapter 3. Results

3.1 Analysis of *App*×*Psen1* double mutant mice

All results were cited from Sato and Watamura et al., 2021.

$App^{NL-F}Psen1^{P117L}$ double-mutant mice produce higher levels of Aβ42 than App^{NL-F} mice

To analyze the combined effect of *App* and *Psen1* mutations on amyloid pathology *in vivo*, I first prepared *App* × *Psen1* double-mutant mice carrying mutations in the endogenous genes. I crossbred $Psen1^{P117L}$ mice [41], produced by using cytosine base editors [68], with App^{NL-F} mice [58] to generate $App^{NL-F/NL-F} \times Psen1^{P117L/WT}$ double-mutant mice ($App^{NL-F}Psen1^{P117L}$ mice).

App^{NL-F} and $App^{NL-F}Psen1^{P117L}$ mice expressed indistinguishable quantities of APP and α/β-CTFs (**Fig. 5a**), suggesting that the P117L mutation does not alter processing of APP by α and β secretases. Consistent with our previous report [58], the Swedish mutations increased the ratio of β/α-CTFs to an identical extent in both lines. I then quantified $Aβ_{40}$ and $Aβ_{42}$ levels in the cortices of App^{NL-F} and $App^{NL-F}Psen1^{P117L}$ mice by Enzyme-Linked Immunosorbent Assay (ELISA). At 3 months of age, male $App^{NL-F}Psen1^{P117L}$ mice produced 22.5-fold GuHCl-soluble (Tris-insoluble) $Aβ_{42}$ compared to App^{NL-F} mice (**Fig. 5b**): female samples showed a similar (26.2-fold) increase. The increase of $Aβ_{40}$ was much smaller, resulting in approximately 11-fold elevation in the $Aβ_{42}/Aβ_{40}$ ratio of male

App^{NL-F}*Psen1*^{P117L} mice compared to *App*$^{NL-F}$ mice (**Fig. 5b**). Female mice showed a similar tendency. In 12-month-old *App*$^{NL-F}$*Psen1*^{P117L} mice, the quantity of Aβ$_{42}$ increased considerably in both Tris-soluble and GuHCl-soluble fractions (**Fig. 5c,d**). Given that the 3-month-old single *Psen1*^{P117L} mice showed only a 2- to 3-fold increase in Aβ$_{42}$ production compared to the wild-type controls [41], these data indicate that the combination of the *App*$^{NL-F}$ and *Psen1*^{P117L} mutations acts on the γ-secretase activity in an additive or synergistic manner.

Figure 5

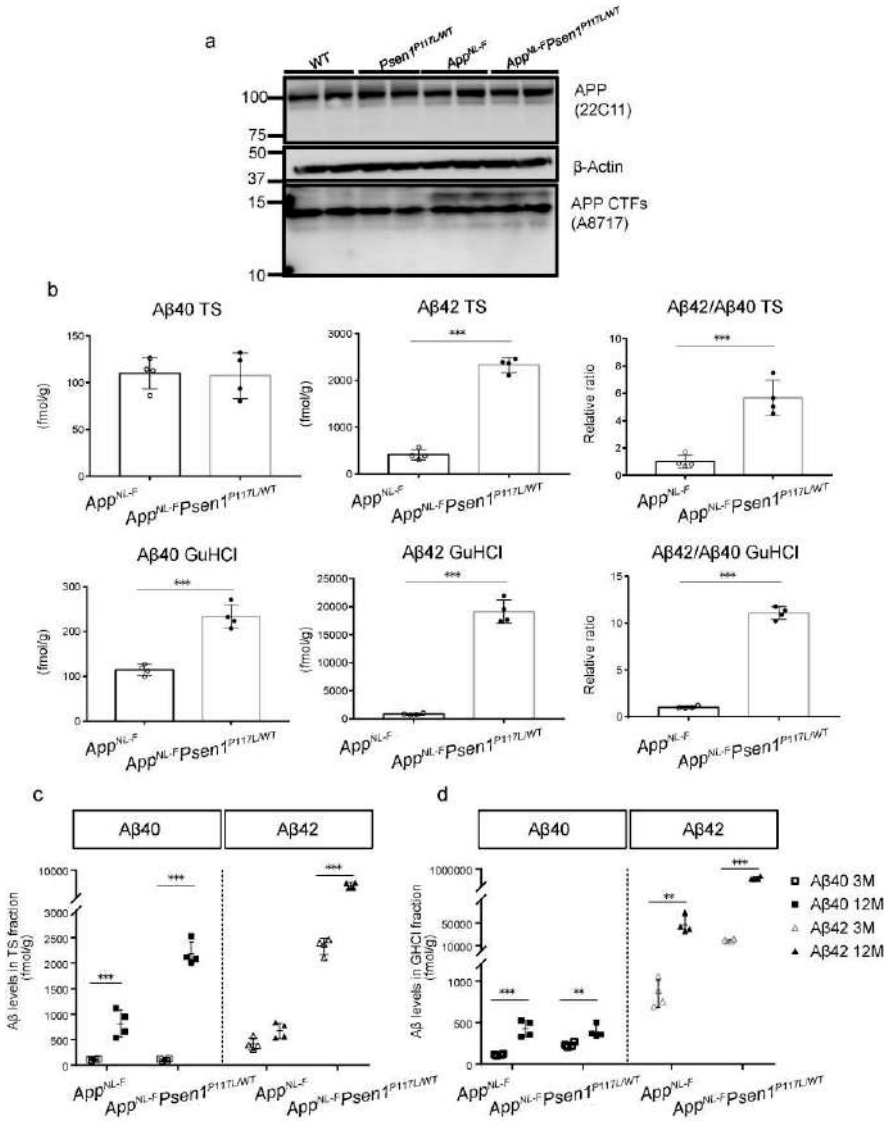

Fig. 5. APP processing and Aβ$_{40}$ and Aβ$_{42}$ production in the brains of *App^{NL-F}Psen1^{P117L}* mice.

(a) APP processing in the cortices of WT, *Psen1^{P117L}*, *App^{NL-F}* and *App^{NL-F}Psen1^{P117L}* mice.

(**b)** Aβ$_{40}$ and Aβ$_{42}$ detected by ELISA from the cortices of 3-month-old *App^{NL-F}* and *App^{NL-F}Psen1^{P117L}* mice. *App^{NL-F}* (n=4) and *App^{NL-F}Psen1$^{P117L/WT}$* (n=4) (Student's t-test).

(**c, d)** Aβ$_{40}$ and Aβ$_{42}$ using Tris-HCl (**c**) and GuHCl (**d**) soluble fractions from 3- and 12-

month-old mice. App^{NL-F} (n=4) and $App^{NL-F}Psen1^{P117L/WT}$ (n=4) (two-way ANOVA followed by Sidak's multiple comparisons test). Each bar represents the mean ± SD. * P < 0.05, ** P < 0.01, *** P < 0.001. These results are cited from Sato et al., *J Biol Chem*. 2021, 297(3):101004.

The *Psen1*^{P117L} mutation also influences Aβ$_{43}$ production

It was previously reported that Aβ$_{43}$ is as pathogenic as Aβ$_{42}$ [82]. I thus performed Aβ$_{43}$ ELISA on cortices from 3- and 12-month-old *App*$^{NL-F}$ and *App*$^{NL-F}$*Psen1*^{P117L} mice. The Tris-soluble, but not insoluble, Aβ$_{43}$ increased more than 2-fold in the brains of *App*$^{NL-F}$*Psen1*^{P117L} mice at 3 months of age compared to *App*$^{NL-F}$ mice (**Fig. 6a,b**). Because I treated the "soluble" fractions with GuHCl before the ELISA measurement [83], soluble oligomers were likely included in these fractions. Aβ$_{43}$ levels in the GuHCl fractions increased with aging both in *App*$^{NL-F}$ and *App*$^{NL-F}$*Psen*^{P117L} mice (**Fig. 6c**). Some *Psen1* mutations such as I213T and R278I result in the overproduction of Aβ$_{43}$ *in vivo* [82, 84]. It is possible that P117L alone or combination with Swedish/Iberian mutations in the *App* gene may lead to an increase in Aβ$_{43}$ by modifying the carboxypeptidase-like activity of γ-secretase in brain [85, 86]. Intriguingly, the Aβ$_{43}$ pathology became more prominent with aging. (See below.)

Figure 6

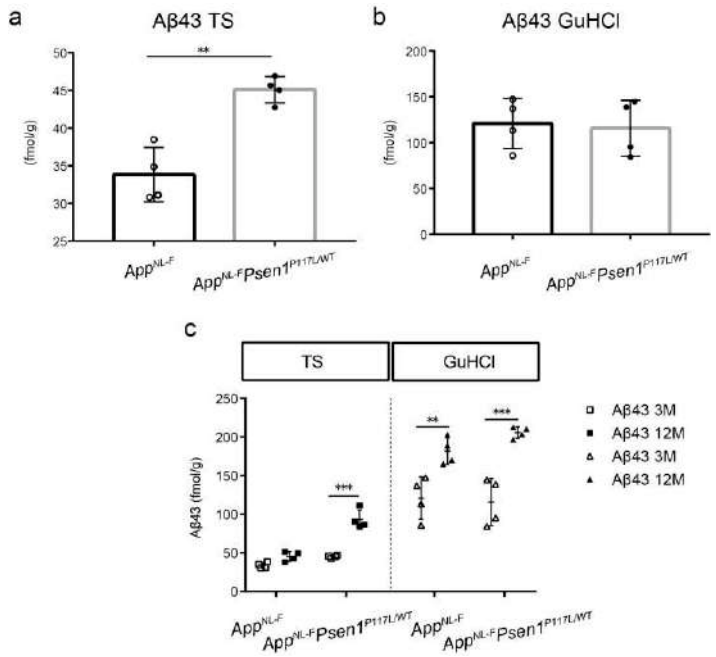

Fig. 6. Aβ$_{43}$ levels detected in the cortices of *App^{NL-F}* and *App^{NL-F}Psen1^{P117L}* mice.

(a,b) Aβ$_{43}$ quantified by ELISA using Tris-HCl (**a**) and GuHCl (**b**) soluble fractions from the cortices of 3-month-old *App^{NL-F}* and *App^{NL-F}Psen1$^{P117L/WT}$* mice. *App^{NL-F}* (n=4) and *App^{NL-F}Psen1$^{P117L/WT}$* (n=4) (Student's t-test). (**c)** Quantity of Aβ$_{43}$ from Tris-HCl and GuHCl soluble fractions from 3- and 12-month-old mice. *App^{NL-F}* (n=4) and *App^{NL-F}Psen1$^{P117L/WT}$* (n=4) (two-way ANOVA followed by Sidak's multiple comparisons test). Each bar represents mean ± SD. * P < 0.05, ** P < 0.01, *** P < 0.001. These results are cited from Sato et al., *J Biol Chem*. 2021, 297(3):101004.

Aβ deposition starts as early as 3 months of age in *App*$^{NL\text{-}F}$*Psen1*^{P117L} mice

I next examined Aβ pathology in the brains of *App*$^{NL\text{-}F}$*Psen1*^{P117L} mice. Immunofluorescence analyses detected Aβ plaques in the cortices of *App*$^{NL\text{-}F}$*Psen1*^{P117L} mice at 3 months of age (**Fig. 7a,b**), whereas *App*$^{NL\text{-}F}$ mice took as long as 6 months to reach an initial and minimal deposition of Aβ [58]. At 12 months, *App*$^{NL\text{-}F}$*Psen1*^{P117L} mice displayed prominent amyloidosis in the cortex and hippocampus comparable to that of *App*$^{NL\text{-}G\text{-}F}$ mice, while significantly fewer Aβ plaques were observed in *App*$^{NL\text{-}F}$ mice (**Fig. 7a-c**). Of note, the number of subcortical plaques in *App*$^{NL\text{-}F}$*Psen1*^{P117L} mice was significantly less than that in *App*$^{NL\text{-}G\text{-}F}$ mice, implying that *App*$^{NL\text{-}F}$*Psen1*^{P117L} mice may recapitulate the human pathology in a more faithful manner [87]. *App*$^{NL\text{-}F}$*Psen1*^{P117L} mice produced dominant deposition of Aβ$_{42}$ with minimal Aβ$_{40}$ (**Fig. 7d**), which is consistent with observations made on *App*$^{NL\text{-}F}$ and *App*$^{NL\text{-}G\text{-}F}$ mice and human samples [58]. Remarkably, I detected a significantly larger number of Aβ$_{43}$-positive plaques in the cortical, hippocampal and subcortical regions of *App*$^{NL\text{-}F}$*Psen1*^{P117L} mice than in those regions of *App*$^{NL\text{-}F}$ and *App*$^{NL\text{-}G\text{-}F}$ mice (**Fig. 7d,e**). These results imply that the Swedish/Iberian and P117L mutations together may accelerate the generation of longer Aβ species including Aβ$_{42}$ and Aβ$_{43}$, resulting in Aβ pathology at younger ages.

Figure 7

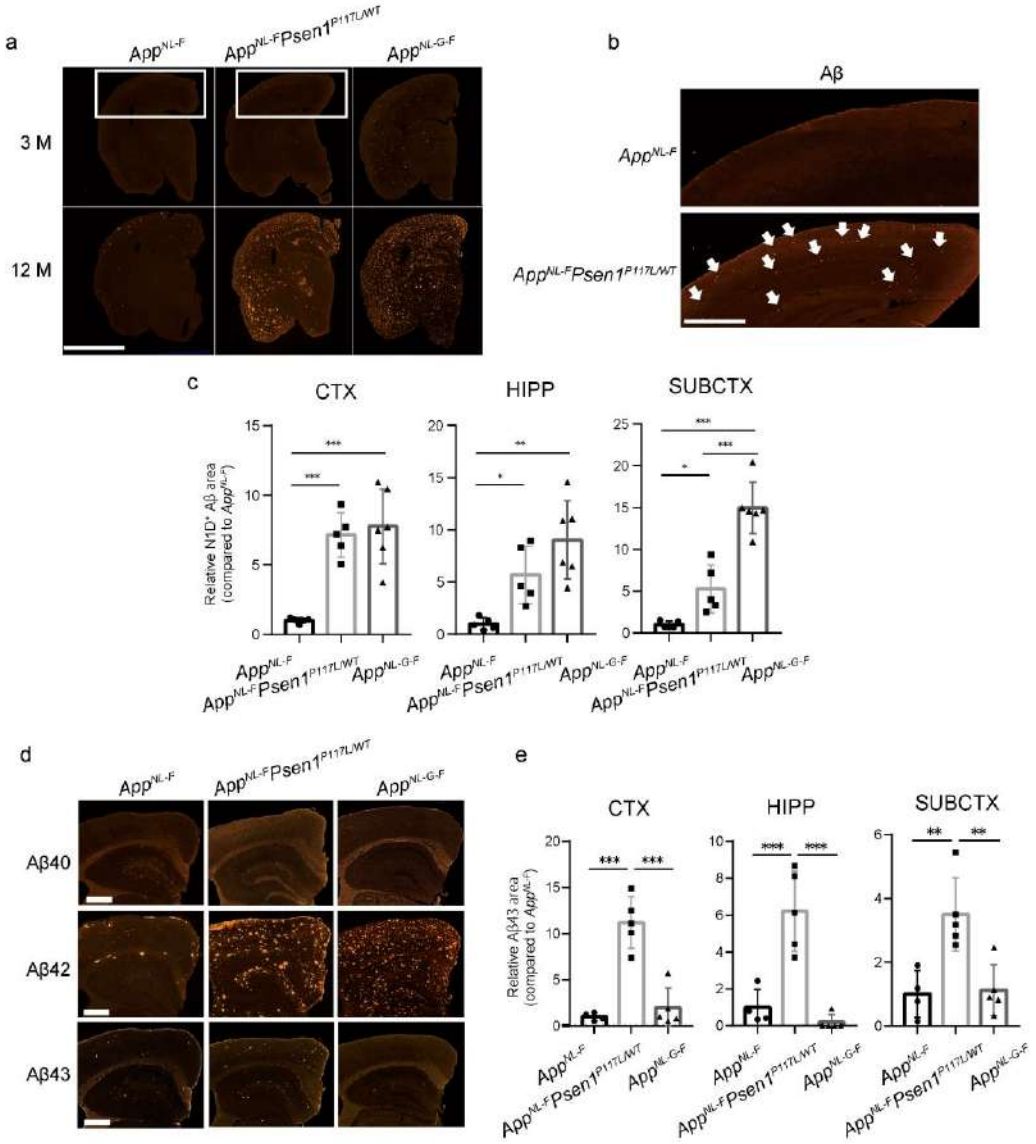

Fig. 7. Aβ plaques deposited in the brains of *App^{NL-F}Psen^{P117L}* mice.

(a) Immunofluorescence images showing amyloid pathology in the brains of 3- (top) and 12-month-old (bottom) *App^{NL-F}*, *App^{NL-F}Psen1$^{P117L/WT}$* and *App^{NL-G-F}* mice. Scale bar represents 2.5 µm. **(b)** High magnification images of tissue sections in (**a**) from 3-month-old animals. Aβ deposition is indicated by white arrows. Scale bar represents 500 µm. **(c)**

N1D-positive areas were quantified in cortical (CTX), hippocampal (HIPP) and subcortical (SUBCTX) regions, respectively. *App*$^{NL-F}$ (n=5), *App*$^{NL-F}$*Psen1*$^{P117L/WT}$ (n=5) and *App*$^{NL-G-F}$ (n=6). (**d)** Sections from 12-month-old mice were immunostained with antibodies specific to Aβ$_{40}$, Aβ$_{42}$ and Aβ$_{43}$. Scale bars represent 50 μm. **(e)** Quantification of Aβ$_{43}$-positive areas in cortical (CTX), hippocampal (HIPP) and subcortical (SUBCTX) regions of 12-month-old mice. *App*$^{NL-F}$ (n=4), *App*$^{NL-F}$*Psen1*$^{P117L/WT}$ (n=5) and *App*$^{NL-G-F}$ (n=5) (one-way ANOVA followed by Tukey's multiple comparisons test). Each bar represents the mean ± SD. * $P < 0.05$, ** $P < 0.01$, *** $P < 0.001$. These results are cited from Sato et al., *J Biol Chem*. 2021, 297(3):101004.

Combination of the Swedish/Iberian and P117L mutations is associated with cored Aβ plaque formation

Several lines of evidence support the notion that diversity in Aβ species correlates with plaque morphology such as typical cored plaques [88-90]. I therefore performed co-staining with N1D antibody raised against $A\beta_{1-5}$ peptide [80] and 1-Fluoro-2,5-bis(3-carboxy-4-hydroxystyryl)benzene (FSB), which recognizes the β-sheet structure within amyloid fibrils and displays higher fluorescence intensity than 1-bromo-2, 5-bis-(3-hydroxycarbonyl-4-hydroxystyryl)benzene (BSB) and Congo red [91], [92]. I observed that FSB-positive signals were positioned at the center of plaques (**Fig. 8a**) and that the N1D/FSB double-positive plaques were significantly increased in the cortex and hippocampus of $App^{NL-F}Psen1^{P117L}$ mice compared to those of App^{NL-F} and App^{NL-G-F} mice (**Fig. 8b**). No significant difference was observed in the subcortical region between $App^{NL-F}Psen1^{P117L}$ and App^{NL-G-F} mice. The frequent presence of classic dense-cored plaques in the cortex of double-mutant mice was confirmed by 3,3'-diaminobenzidine (DAB) staining (**Fig. 8c**).

Figure 8

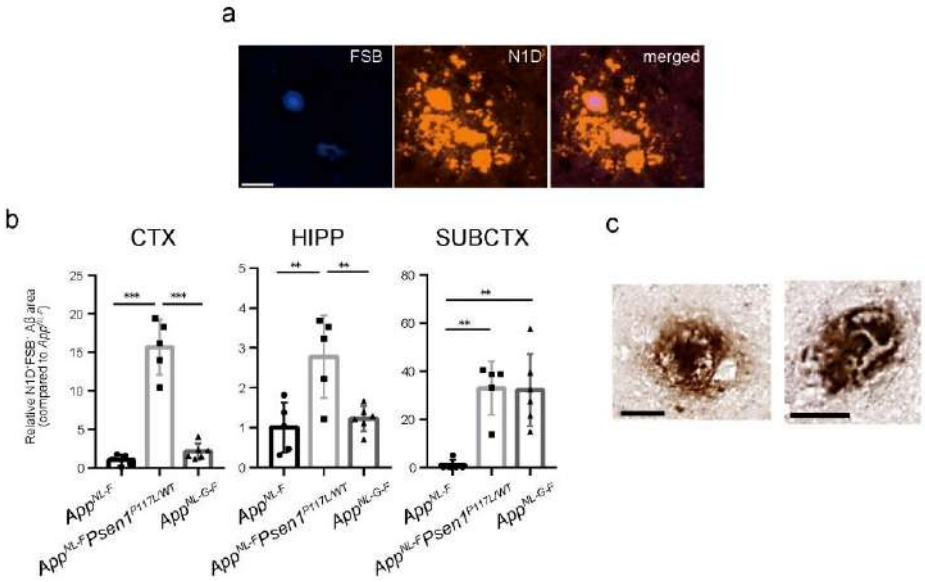

Fig. 8. Aβ plaques with a cored structure in *App^{NL-F}Psen1^{P117L}* mice.

(a) Brain sections from 12-month-old *App^{NL-F}Psen1$^{P117L/WT}$* mice were co-stained with FSB and N1D antibody. (**b)** FSB/N1D double-positive areas were quantified in the brains of *App^{NL-F}*, *App^{NL-F}Psen1$^{P117L/WT}$* and *App^{NL-G-F}* mice. *App^{NL-F}* (n=5), *App^{NL-F}Psen1$^{P117L/WT}$* (n=5) and *App^{NL-G-F}* (n=6) (one-way ANOVA followed by Tukey's multiple comparisons test). Each bar represents mean ± SD. * $P < 0.05$, ** $P < 0.01$, *** $P < 0.001$. **(c)** Representative images of dense-core plaques surrounded by a halo effect detected by DAB staining. Scale bars represent 25 μm. These results are cited from Sato et al., *J Biol Chem*. 2021, 297(3):101004.

Neuroinflammation is elevated in *App^{NL-F}Psen1^{P117L}* mice, particularly in the hippocampus.

Neuroinflammation surrounding Aβ plaques manifests as one of the pathological features in AD patients [58, 93, 94], and Genome-Wide Association Studies (GWAS) have suggested etiological involvement of neuroinflammation in AD development[95-97]. I thus analyzed the neuroinflammatory status of three mouse lines (*App^{NL-F}*, *App^{NL-F}Psen1^{P117L}* and *App^{NL-G-F}*) by immunofluorescence using antibodies against Aβ (82E1), microglia (anti-Iba1) and astrocytes (anti-GFAP). I confirmed the presence of glial cells surrounding Aβ plaques in *App^{NL-F}Psen1^{P117L}* mice (**Fig. 9a,b**). Consistent with our previous reports, single *App^{NL-G-F}*-KI mice rather than *App^{NL-F}*-KI mice exhibit robust microgliosis and astrocytosis accompanying progressive amyloidosis [58, 59]. Quantification of immunofluorescence images indicated that more neuroinflammation was evident in *App^{NL-F}Psen1^{P117L}* and *App^{NL-G-F}* than *App^{NL-F}* mice (**Fig. 9c**). This was somewhat predictable because *App^{NL-F}Psen1^{P117L}* and *App^{NL-G-F}* mice accumulate more pathological Aβ than *App^{NL-F}* mice (**Fig. 3a-c)**. A unique observation is that *App^{NL-F}Psen1^{P117L}* mice exhibited significantly greater microgliosis and astrocytosis than *App^{NL-G-F}* mice in the hippocampus despite the indistinguishable levels of Aβ amyloidosis therein. This phenomenon may be associated with increased $A\beta_{43}$ deposition (**Fig. 3d,e**) and cored plaques in *App^{NL-F}Psen1^{P117L}* mice (**Fig. 8a,b**), but these speculations alone

cannot fully account for the neuroinflammation that took place selectively in the hippocampus. In any case, these findings indicate that *App*$^{NL\text{-}F}$*Psen1*^{P117L} mice may be suitable for investigating hippocampal neuroinflammation.

Figure 9

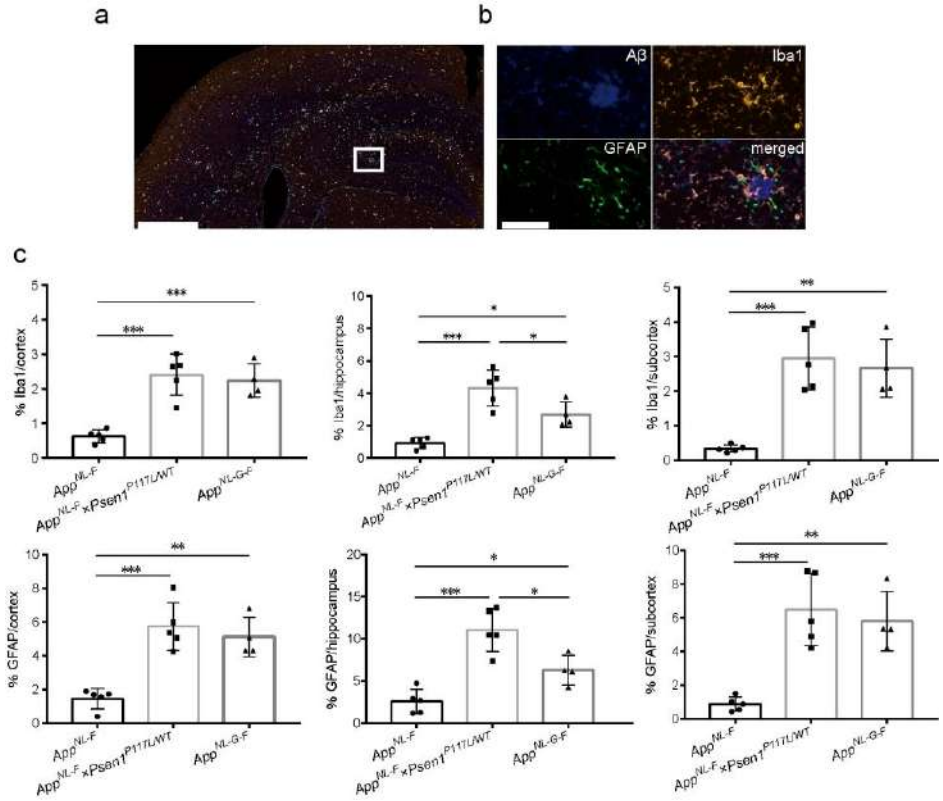

Fig. 9. Glial responses in *App*$^{NL\text{-}F}$*Psen1*$^{P117L/WT}$ mouse brain. (a) Inflammatory signals were detected with GFAP and Iba1 antibodies using brain sections from 12-month-old *App*$^{NL\text{-}F}$*Psen1*$^{P117L/WT}$ mice. Aβ pathology was detected by immunostaining with 82E1 antibody. Scale bar represents 500 μm. (**b)** Higher magnification image of the area marked in white in (**a**). Scale bar represents 50 μm. (**c)** Immunoreactive areas of GFAP or Iba1 were quantified in the brains of *App*$^{NL\text{-}F}$, *App*$^{NL\text{-}F}$*Psen1*$^{P117L/WT}$ and *App*$^{NL\text{-}G\text{-}F}$ mice. Each bar represents the mean ± SD. * $P < 0.05$, ** $P < 0.01$, *** $P < 0.001$, *App*$^{NL\text{-}F}$ (n=5), *App*$^{NL\text{-}F}$*Psen1*$^{P117L/WT}$ (n=5) and *App*$^{NL\text{-}G\text{-}F}$ (n=4) (one-way ANOVA followed by Tukey's multiple comparisons test). These results are cited from Sato et al., *J Biol Chem*. 2021,

297(3):101004.

3.2 Analysis of *App* knock-in mice devoid of Swedish mutation

Generation of $App^{G\text{-}F}$ and $App^{huA\beta}$ Mice By CRISPR/Cas9

Saito and colleagues previously developed $App^{NL\text{-}G\text{-}F}$ mice by manipulation of the mouse *App* gene using a knock-in strategy [58]. Exon 16 of the *App* gene contains the Swedish mutations (KM670/671NL) while exon 17 contains the Arctic and Beyreuther/Iberian mutations (**Fig. 10A**). Firstly, single-guide RNA (sgRNA)-App-Exon16 and single-stranded oligodeoxynucleotide (ssODN) containing the WT sequence to substitute the Swedish mutations (NL670/671KM) together with Staphylococcus aureus Cas9 (SaCas9) mRNA, where the proto-spacer adjacent motif (PAM) sequence is required as NNGRRT, were injected into the cytoplasm of heterozygous zygotes of $App^{NL\text{-}G\text{-}F}$ mice. The PAM sequence overlapped with the Swedish mutations so that, when knock-in of the WT sequence occurred, it could prevent sequential cleavages by SaCas9 because the original PAM site had disappeared (**Fig. 10A,B**). Sanger sequencing analysis revealed that the desired substitution via homology-directed repair occurred successfully in the $App^{NL\text{-}G\text{-}F}$ allele of the founder mice with an efficiency of 10.8％ (**Fig. 10C**). Crossing the founder mice with WT mice to generate F1 mice, I confirmed that the Swedish mutations were fully removed from the $App^{NL\text{-}G\text{-}F}$ allele (**Fig. 10C**). Using an identical strategy in App^{NL} zygotes (see methods), I also generated $App^{huA\beta}$ mice that carry only the

humanized Aβ sequence without any familial AD-causing mutation. I confirmed that there were no unexpected mutations in exons 16, 17 and 18 of the *App* gene in $App^{G\text{-}F}$, $App^{huA\beta}$ mice and others (**Fig. S1**), indicating that all these lines are isogenic. $App^{G\text{-}F/wt}$ mice were then intercrossed to obtain homozygous $App^{G\text{-}F/G\text{-}F}$ mice that were viable. To explore the off-target effects of CRISPR/Cas9-mediated genome editing in the founder mice, I searched for potential off-target sites using the online tool COSMID [76] and Cas-OFFinder [77] (**Fig. 10D**). Targeted sequencing analysis focusing on the candidate genomic regions revealed that no off-target modification took place in the founder mice of $App^{G\text{-}F}$ and $App^{huA\beta}$ mice.

Figure 10

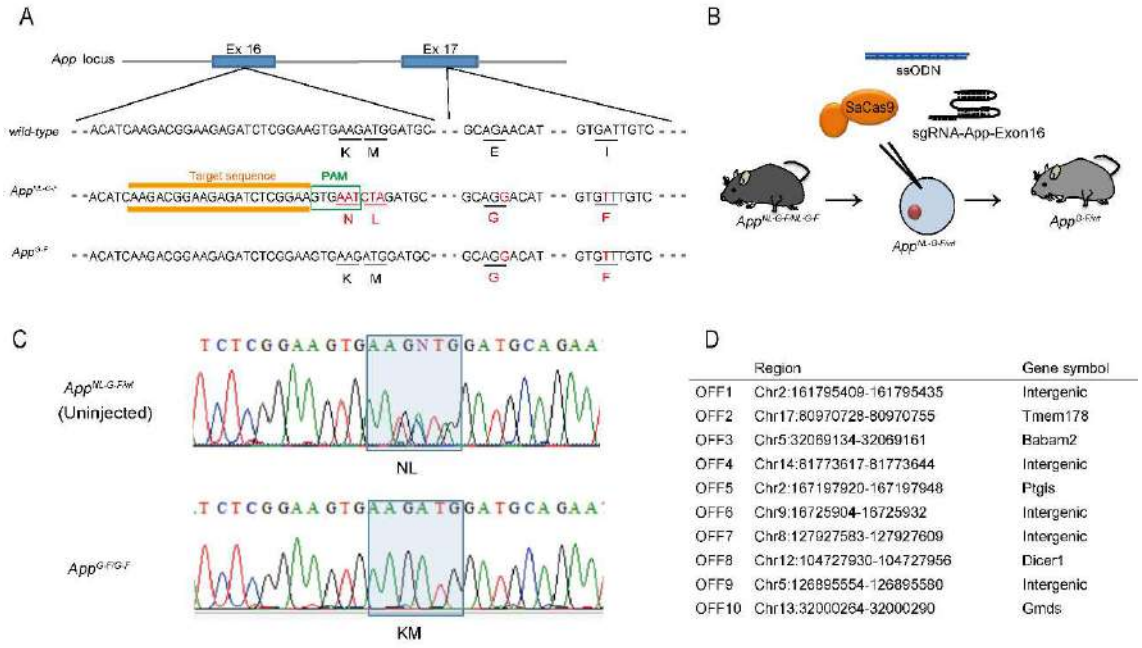

	Region	Gene symbol
OFF1	Chr2:161795409-161795435	Intergenic
OFF2	Chr17:80970728-80970755	Tmem178
OFF3	Chr5:32089134-32089161	Babam2
OFF4	Chr14:81773617-81773644	Intergenic
OFF5	Chr2:167197920-167197948	Ptgis
OFF6	Chr9:16725904-16725932	Intergenic
OFF7	Chr8:127927583-127927609	Intergenic
OFF8	Chr12:104727930-104727956	Dicer1
OFF9	Chr5:126895554-126895580	Intergenic
OFF10	Chr13:32000264-32000290	Gmds

Fig, 10. Generation of the single *App*$^{G-F}$ knock-in mice

(A) Exact sequences showing sgRNA (orange) with the PAM site (green) in the mouse *App* gene. Red characters represent the Swedish (KM670/671NL), Arctic (E693G) and Beyreuther/Iberian (I716F) mutations, respectively. (B) Schematic illustration of CRISPR/Cas9-mediated genome editing in *App*$^{NL-G-F}$ knock-in mouse zygotes by microinjection. (C) Sanger sequencing results determined *App*$^{NL-G-F/wt}$ (upper panel) and *App*$^{G-F/G-F}$ genotype (lower panel). The desired mutation loci (NL670/671KM) are indicated as a rectangular shape in blue shading. See also Figure S1. (D) Regional information of potential off-target sites which were identified using Cas-OFFinder (http://www.rgenome.net/cas-offinder/) and COSMID (https://crispr.bme.gatech.edu/).

Neuropathology of *App*$^{G-F}$ Mice

I next analyzed the extent of amyloid pathology in the *App*$^{G-F}$ mice. Aβ$_{42}$ levels in the cortex were age-dependently increased in the Tris-HCl and Guanidine-HCl (GuHCl) soluble fractions, with Aβ$_{40}$ levels remaining relatively stable (**Fig. 11A,B**). I also observed that progressive amyloid pathology mainly in the cortex and hippocampus occurred in an age-dependent manner (**Fig. 11C,D**). Initial deposition of Aβ was observed around 4 months of age in the *App*$^{G-F}$ mice. At 12 months, Aβ deposition in the brains of *App*$^{G-F}$ mice detected in a much larger area than that in the *App*$^{NL-F}$ mice, but at a lower level to that in *App*$^{NL-G-F}$ mice (**Fig. S2**). In addition, I analyzed the Aβ species constituting amyloid plaques in the *App*$^{G-F}$ mice using N-, C-terminal (Aβ$_{40,}$ Aβ$_{42}$) and Aβ$_{3(pE)-X}$ (pE: pyroglutamate) specific antibodies. Aβ$_{40,}$ Aβ$_{42}$ and Aβ$_{3(pE)-X}$ species were detected in the brain with a predominant deposition of Aβ$_{42}$ over Aβ$_{40}$ (**Fig. 11E**). These results are consistent with the neuropathology observed in sporadic AD patients and in *App*$^{NL-F}$and *App*$^{NL-G-F}$ mice [58].

Chronic inflammation surrounding Aβ plaques in the brain is a pathological hallmark of AD. I therefore investigated the status of glial cells surrounding amyloid plaques in the *App*$^{G-F}$ mice. Reactive astrocyte and activated microglia are pathological signs of neuroinflammation, with evidence of both being observed (**Fig. 11F**). I also examined pre- and post-synaptic alterations in brain slices and detected loss of synaptophysin and

PSD-95 immunoreactivity near the Aβ plaques, which is consistent with those in other *App* knock-in mice (**Fig. 11G**) [58].

Figure 11

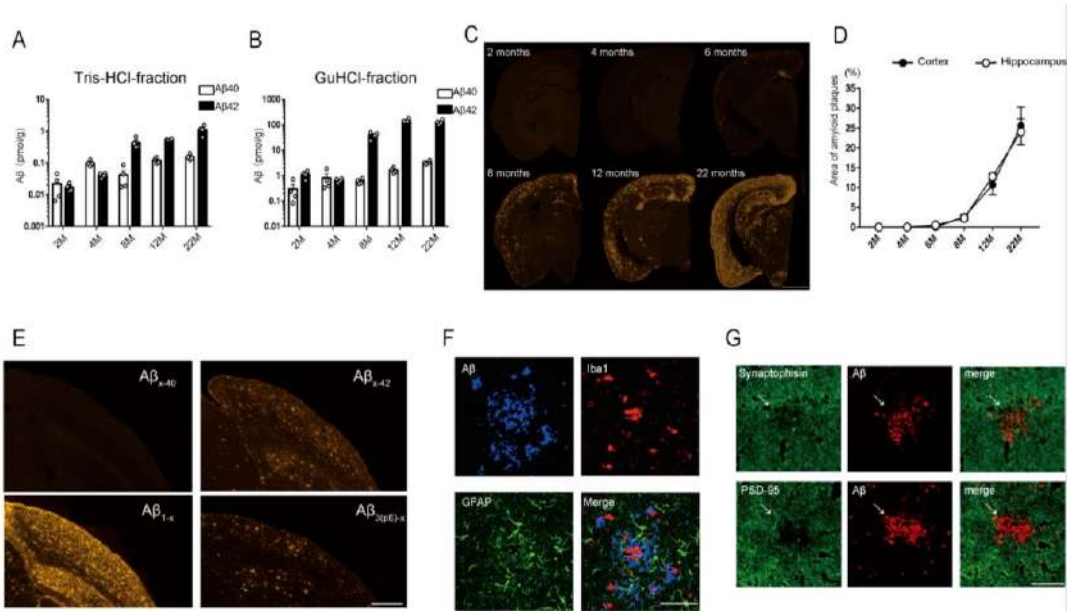

Fig. 11. Neuropathology of *App*$^{G\text{-}F}$ mice

(A-B) Aβ content detected by ELISA using Tris-HCl soluble fraction (A) and GuHCl soluble fraction (B) of the cortices of *App*$^{G\text{-}F}$ mice at 2- 4-, 8-, 12- and 22 months (n=4 at each time point). Each bar represents the mean ± SEM. (C) Immunohistochemistry images showing Aβ deposition as indicated by immunostaining with N1D antibody against $A\beta_{1-5}$. Scale bars indicate 1 mm. (D) Quantitative analysis of amyloid plaque areas in the cortices and hippocampi of *App*$^{G\text{-}F}$ mice at 2-, 4-, 8- and 12 months (n=4 at each time point) and at 22 months (n=3). Each bar represents the mean ± SEM. (E) Specific antibodies against N- ($A\beta_{1\text{-}x}$ and $A\beta_{3(pE)\text{-}x}$) and C- ($A\beta_{x\text{-}40}$ and $A\beta_{x\text{-}42}$) terminus of Aβ reveal the deposition of each species of Aβ in the brains of 22-month-old *App*$^{G\text{-}F}$ mice. Scale bars represent 500 μm. (F) Inflammatory responses in the cortices of *App*$^{G\text{-}F}$

mice at 22 months. Astrocytes (green) and microglia (red) can be seen surrounding Aβ (blue), as detected by triple staining with antibodies against GFAP, Iba1 and the N-terminus of human Aβ (82E1), respectively. Scale bars represent 100 μm. (G) Synaptic alteration detected in the hippocampus of a 22-month-old $App^{G\text{-}F}$ mouse. Aβ detected by 4G8 antibody against $A\beta_{17–24}$ was double stained with synaptophysin antibody as a presynaptic marker or with PSD95 antibody as a postsynaptic marker. White arrows indicate synaptic loss near Aβ aggregation. Scale bars represent 25 μm.

Assessment of BACE1 Inhibition in *App*$^{G-F}$ Mice

The Swedish mutations have been considered to underlie the decreased APP processing potency of β-secretase inhibitors. Previous studies have shown that β-secretase inhibition is less efficacious in cells stably overexpressing *APP*-containing Swedish mutations than from cells transfected with wild-type APP [98, 99]. To compare the potency of β-secretase inhibition in animal models – with or without Swedish mutations in the *APP* gene – not relying on the overexpression paradigm, I administrated verubecestat, a potent BACE1 inhibitor, to 3-month-old WT, *App*$^{NL-G-F}$ and *App*$^{G-F}$ mice following a previously reported experimental protocol [81]. I found that a single oral administration of verubecestat at the dose of 10 mg/kg significantly reduced both $A\beta_{40}$ and $A\beta_{42}$ levels in the cortices of *App*$^{G-F}$ mice, but not in *App*$^{NL-G-F}$ mice, 3 hours after treatment (**Fig. 12A-D**). These results indicate that the Swedish mutations are responsible for the poor potency of BACE1 inhibitors *in vivo* and that *App*$^{G-F}$ mice could serve as a powerful tool for the precise characterization of BACE1 and candidate inhibitory compounds.

Figure 12

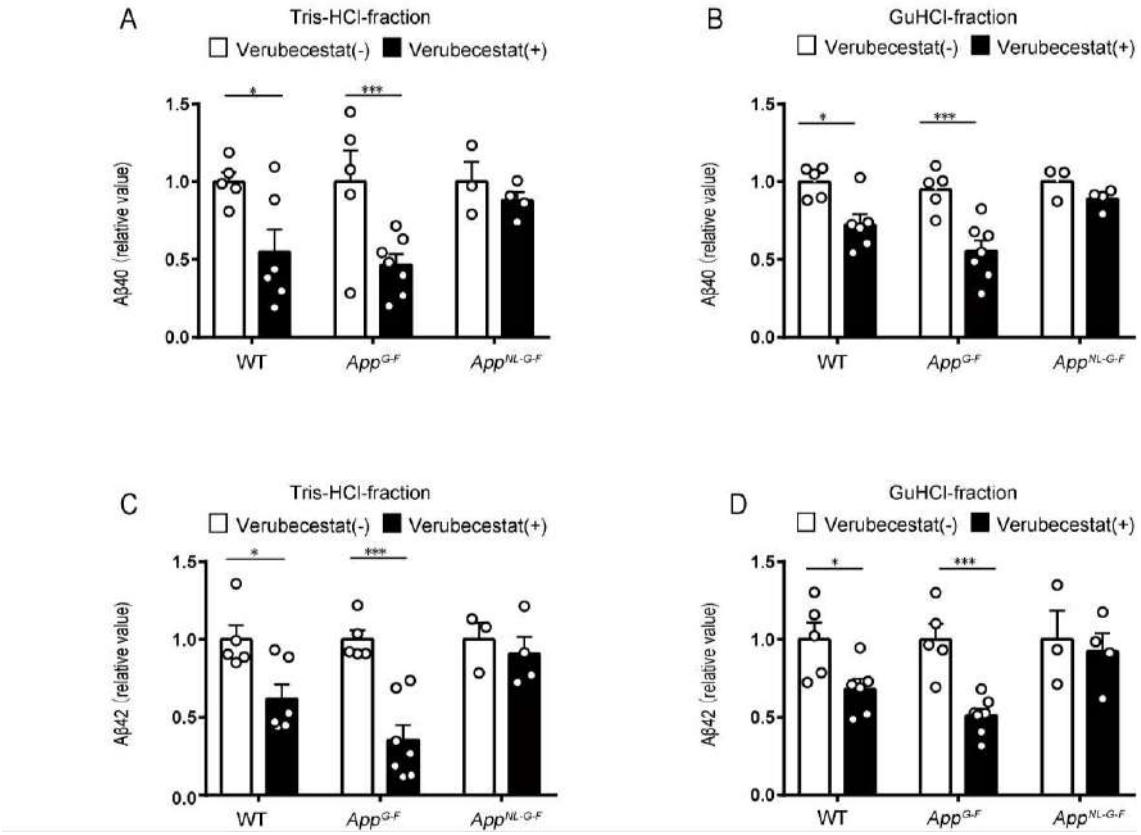

Fig. 12. Removal of the Swedish mutations rescues the BACE1 inhibitory effect of verubecestat

(A-D) $A\beta_{40}$ and $A\beta_{42}$ levels detected by ELISA were decreased both in the Tris-HCl fraction (A, C) and GuHCl fraction (B, D) of 3-month-old wild-type and App^{G-F} mice, but not in App^{NL-G-F} mice. The differences in Aβ quantity between strains were detected as expected in untreated mice. Each bar represents the mean ± SEM. * $P < 0.05$, ** $P < 0.01$, *** $P < 0.001$. (WT; verubecestat (+) n=5, (-) n=6, App^{G-F}; (+) n=5, (-) n=7 and App^{NL-G-F}; (+) n=3, (-) n=4, Student's t-test).

Relationship Between the Quantity of CTF-β and Endosomal Abnormality *in vivo*

Several studies have reported that the Swedish mutations alter the APP processing and shift the processing towards an amyloidogenic pathway via competitive behavior of α- and β-secretases [39, 100]. In an earlier study, we showed that the ratio of CTF-β/α levels in $App^{NL-F}$and App^{NL-G-F} mice is higher than that in wild-type mice [58]. Here, I used five different *App* knock-in lines and WT mice to examine the effect of the mutations on the quantity of CTF-β and the extent of endosomal dysfunction. The ratio of CTF- β/α in App^{G-F} mice was much lower compared to App^{NL}, App^{NL-F} and App^{NL-G-F} mice with no alteration of APP levels (**Fig. 13A and S3**). This finding indicates a slight shift to the β-cleavage pathway. I next examined whether CTF-β affects endosomal function *in vivo*. Some groups suggest that accumulated CTF-β itself induces endosome abnormalities independent of Aβ toxicity [49, 73]. The quantity of CTF-β in the brains of App^{G-F} mice was comparable to that of WT controls (**Fig. 13A-B**). I focused on early endosomal antigen 1 (EEA1) as an early endosome marker and performed immunohistochemical analyses of the hippocampal CA1 region in the six mouse lines: WT, $App^{huA\beta}$, App^{NL}, App^{NL-F}, App^{G-F} and App^{NL-G-F} knock-in mice. I detected a significant increase in the mean $EEA1^{+}$ area in the CA1 pyramidal cell layer of the five mutant lines compared with that of WT mice (**Fig. 13C-D**). Kwart *et al*. demonstrated that endosome enlargement is a common pathology in familial APP mutant iPSC neurons, and that the quantity of CTF-

β correlates with endosome abnormality. I consistently observed a significant alteration of the distribution of endosome size in the five mutant mouse lines, including *App*$^{huA\beta}$ knock-in mice, compared with that of wild-type mice (**Fig. 13E**). This was seen as an increase in the ratio of larger endosomes (>1 μm^2) and a decrease in the ratio of smaller endosomes (<0.5 μm^2) (**Fig. 13E**). However, CTF-β levels did not correlate with endosome enlargement. Of note, endosomal sizes were enlarged in the brains of *App*$^{G\text{-}F}$ mice, the extent of which was similarly observed in *App*$^{NL\text{-}G\text{-}F}$ mice irrespective of the large differences in CTF-β levels (**Fig. 13B-F**). I sequenced the C-terminal region of APP in *App* knock-in mouse lines and excluded the possibility that unexpected mutation was causing this alteration (**Fig. S1**). These findings suggest that early endosomal enlargement might be caused by not only excessive CTF-β but also by other toxic agents including human Aβ secretion in mouse brains.

Figure 13

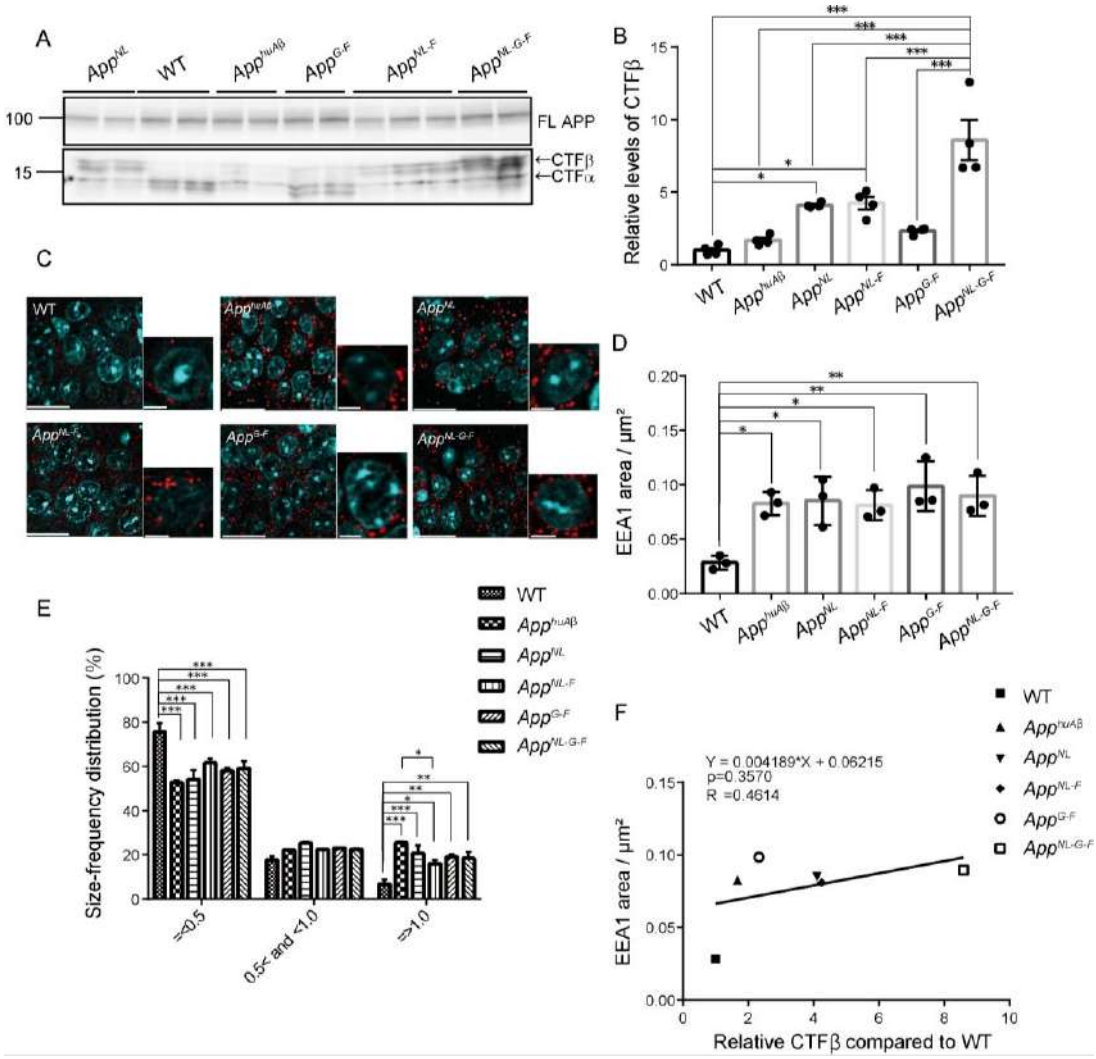

Figure 13. APP CTF expression levels and endosome abnormalities

(A) APP CTF expression in the brains of 12-month-old WT, *App*$^{huA\beta}$, *App*^{NL}, *App*$^{NL-F}$, *App*$^{G-F}$ and *App*$^{NL-G-F}$ mice. See also **Figures S3**. (B) Quantification of relative levels of APP CTF-β relative levels compared to WT. WT, *App*$^{huA\beta}$, *App*^{NL}, *App*$^{NL-F}$, *App*$^{G-F}$ and *App*$^{NL-G-F}$; n=4 for each genotype, one-way ANOVA followed by Tukey's multiple comparison test. (C) Immunohistochemical images of early endosomes in CA1 pyramidal

cells detected by EEA1 antibody (red) and Hoechst33342 staining of nuclei (blue). Brain sections from 12-month-old WT, $App^{huA\beta}$, App^{NL}, App^{NL-F}, App^{G-F} and App^{NL-G-F} mice. Scale bars indicate 20 μm (left) and 5 μm (right), respectively for each genotype. (D) Statistical analysis of $EEA1^{+}$ area per μm^2 in pyramidal cells of hippocampal CA1 region. (E) Endosomal size distribution was statistically analyzed using MetaMorph imaging software. WT, $App^{huA\beta}$, App^{NL}, App^{NL-F}, App^{G-F} and App^{NL-G-F}; n=3 for each genotype, one-way ANOVA followed by Tukey's multiple comparison test (D and E). Each bar represents the mean ± SEM. * $P < 0.05$, ** $P < 0.01$, *** $P < 0.001$ (B, D and E). (F) Relationship between EEA1 area / μm^2 and CTF-β content. Pearson's correlation coefficient R, the associated p value and linear regression equation are shown in the figure.

Chapter 4. Discussion

4.1 *App*×*Psen1* double-mutant mice with early deposition of wild-type human Aβ

The primary aim of the present study was to generate *App* knock-in mice that pathologically accumulate wild-type human Aβ devoid of the Arctic mutation. $App^{NL\text{-}G\text{-}F}$ mice carrying the Arctic mutation exhibit the most rapid and aggressive pathology among all the *App* knock-in mice that had been created. My motivation was based on the undesirable nature of the Arctic mutation that impedes the physiological metabolism and clearance of Aβ [57, 101], thus making it difficult to study etiological processes upstream of Aβ deposition. Arctic Aβ also binds to anti-Aβ antibodies raised against Aβ peptide in a distinct manner [58], making $App^{NL\text{-}G\text{-}F}$ mice unsuitable for preclinical immunotherapy studies. The generation of *App* knock-in mice that accumulate wild-type human Aβ without the Arctic mutation as early as $App^{NL\text{-}G\text{-}F}$ mice is therefore a prerequisite before disease-modifying strategies targeting mechanisms upstream of Aβ deposition can be developed.

Introduction of the $Psen1^{P117L}$ mutation into $App^{NL\text{-}F}$ mice resulted in an unexpected acceleration of $A\beta_{42}$ and $A\beta_{43}$ deposition. Although the numbers of cortical and hippocampal plaques visualized by an antibody specific to the N-terminus of Aβ (N1D)

were indistinguishable between *App*$^{NL\text{-}G\text{-}F}$ and *App*$^{NL\text{-}F}$*Psen1*^{P117L} mice, *App*$^{NL\text{-}F}$*Psen1*^{P117L} mice showed a larger number of cored plaques in the cortex and hippocampus, and more gliosis in the hippocampus than was seen in *App*$^{NL\text{-}G\text{-}F}$ mice. Mechanisms accounting for these observations are unclear but may be associated with the prion-like nature of $A\beta_{43}$ [102]. In any case, the *App*$^{NL\text{-}F}$*Psen1*^{P117L} mice may become a useful tool for examining the roles of hippocampal neuroinflammation in the etiology of AD.

Other groups have also attempted to combine the *App* and *Psen1* mutations. Flood *et al.* generated double knock-in mice that harbored the Swedish mutations in the *App* gene and the P264L/P264L mutation in the *Psen1* gene [103]. These mice showed elevation of $A\beta_{42}$ levels and pathological amyloidosis without overexpression of APP. Although this model has seldom been used in the research community presumably because the progression of pathology was too slow and mild, both their group and ours share similar ideas and goals. Similarly, Li *et al.* generated a mouse model of cerebral amyloid angiopathy（CAA）[104]. I observed only a few CAA-like structures (less than 10 per hemisphere) mainly in meninges in the 12-month-old *App*$^{NL\text{-}F}$*Psen1*^{P117L} mice, indicating that this is parenchymal amyloidosis-dominant model. Typical images of CAA are shown in **Fig. S4**.

However, unlike the models generated by Flood *et al.* and Li *et al.*, the 3rd generation

model mice are heterozygous for the *Psen1* mutation, making them more difficult to breed in many labs. Moreover, I must point out that $App^{NL\text{-}F}Psen1^{P117L}$ mice are probably inadequate for studying β- and γ-secretases and their modifiers because the cleavages catalyzed by these secretases are artificially altered by the mutations. I thus expect the mutant mice to become more suitable for the examining catabolism and clearance of Aβ than its anabolism. This makes agonist(s) for somatostatin receptor subtype(s) a medication candidate for treatment of preclinical AD [105]. I will share these mice with the AD research community to accelerate the fight against the disease that deprives patients of their human dignity.

4.2 *App* knock-in mice devoid of Swedish mutation confer differential mode of β-secretase inhibitor action and endosomal abnormalities

In the present study, by removing the Swedish mutation from $App^{NL\text{-}G\text{-}F}$ mice, I developed a new *App* knock-in line, $App^{G\text{-}F}$, which harbors both the Arctic and Beyreuther/Iberian mutations. The $App^{G\text{-}F}$ mice exhibited an age-dependent and typical amyloid pathology, neuroinflammation, characterized by reactive astrocytes and activated microglia surrounding the Aβ plaques, and aberrant pre- and post-synaptic structures near the plaques. Verubecestat intervention effectively reduced Aβ levels in the cortices of $App^{G\text{-}F}$ mice, but not in the conventional *App* knock-in mice containing the Swedish mutation. Endosomal enlargement was also observed, although the CTF-β levels in the brains of $App^{G\text{-}F}$ mice were comparable to those of WT mice.

Aβ deposition in the brains of $App^{G\text{-}F}$ mice occurs from around 4 months of age, compared to around 2 months of age in $App^{NL\text{-}G\text{-}F}$ mice and 6 months in $App^{NL\text{-}F}$ mice [58], suggesting that the $App^{G\text{-}F}$ mice serve as "a moderate model" of the three lines from the point of view of amyloidosis in the mouse brain (**Figure S2**). $App^{G\text{-}F}$ mice also showed an age-dependent amyloid pathology in the subcortical area as well as in the cortex and hippocampus, which is consistent with human carriers of the Arctic mutation [106]. This is the first AD mouse model that recapitulates amyloid pathology in the brain, but does not harbor the Swedish mutation and is not dependent on APP overexpression.

Previous studies based on transgenic mice overexpressing the *APP* gene with familial mutations and CRISPR/Cas9-mediated genomic modified iPSCs indicated that AD-associated early endosomal enlargement depends on the excess accumulation of CTF-β, but not Aβ [49, 73, 107-111]. On the other hand, other studies have reported that Aβ toxicity is indeed a causative factor for the impaired endocytic sorting [112-114]. In this study, using *App* knock-in mice, I observed early endosomal abnormalities in hippocampal CA1 pyramidal neurons both with or without CTF-β overproduction compared to WT mice (**Fig. 13 and S3**). Given that $A\beta_{42}$ levels reached a plateau and that Aβ plaque formation was spread abundantly in the hippocampi of $App^{G\text{-}F}$ mice as young as 12 months of age (**Fig. 11A,B**), Aβ species themselves, independent of CTF-β accumulation, are also likely to cause early endosomal enlargement *in vivo*. Future analyses on concerning which Aβ peptide(s) such as $A\beta_{40}$, $A\beta_{42}$, $A\beta_{3(pE)\text{-}X}$ are responsible for altering the endocytic system are required to elucidate the underlying mechanism(s). These results show that humanization of Aβ alone induces endosomal enlargement in mice, which is consistent with a transcriptomic study using weighed gene co-expression network analysis (WGCNA) indicating that Eea1 is one of the highly correlated genes explaining biological alterations in the hippocampi of huAβ-KI mice [115]. On the other hand, recent studies indicate that endosomal enlargement occurs via an APP-independent

pathway [116], [117]. Taken together, endosomal trafficking defects associated with AD cytopathogenesis may occur via different means such as CTF-β-dependent, Aβ-dependent and APP-independent pathways.

A large number of BACE1 inhibitors have been explored and investigated as potent disease-modifying drugs in the AD research field, but all of them, to my knowledge, have failed to show efficacy in clinical trials. However, as the A673T (Icelandic) mutation[45] positively established the proof-of-concept that the inhibition of β-secretase cleavage reduces the risk of AD onset, the discovery of BACE1 inhibitory compounds that pass through the blood-brain barrier and directly abrogate Aβ production in human brains remains a promising path to treat AD patients. Although single App^{NL-F} or App^{NL-G-F} knock-in mice have been used in more than 500 laboratories and pharmaceutical companies worldwide as second-generation mouse models of AD [58], these mice are not compatible with BACE1-related studies due to the presence of Swedish mutations. These results provide consistent evidence that the Swedish mutations hinder the BACE1 inhibitory activities of verubecestat *in vivo*, similar to several reports showing the reduced activity of BACE1 inhibitors including not just verubecestat [98] but also other drug candidates in mice harboring the Swedish mutations [118], [39]. Thus, App^{G-F} mice now profile as a novel type of single *App*-KI mice without the interference of the Swedish

mutations. The potential exists for these mice to be used to efficiently and precisely to identify active compounds for BACE1 inhibition *in vivo* that might have been overlooked in a vast number of studies in which AD model mice were used that contained the Swedish mutations and were based on an APP overexpression paradigm. Expanded range of single *App* knock-in mice including the $App^{NL\text{-}F}$, $App^{NL\text{-}G\text{-}F}$ and $App^{G\text{-}F}$ lines, are available for use by research groups and companies who can choose the AD mouse model line most suited to the purpose of their studies. It should be noted that, no matter their age, these are just preclinical models against amyloidopathology alone, because these models cannot recapitulate tau pathology and neuronal degeneration. We should be aware that what we see using *App* knock-in mice focuses on only a few aspects of AD pathophysiology.

Chapter 5. Conclusion

As is well known, especially for complex disorders that progress with aging including AD, it is the most critical to determine ‘when’ we intervene in a disease with medications and ‘when’ we evaluate the drug efficacy in clinical trials. Recent clinical studies have focused on how quickly we start to treat Aβ long before cognitive symptoms appear. Aβ deposition initiates more than 20 years before the onset, which thus forces pharmaceutical companies to be patient and makes them hard to decide what primary endpoints will be before trials begin. The difficulty in AD drug development has been easy to imagine as the success rate for AD trials during the 2002 to 2012 was 0.4% while 19.8% for oncology field [119]. What makes these different outcomes? These unfortunate facts can be contributed by so many factors, but this thesis focused on AD mouse models that play an essential role in nonclinical studies.

Before new drug candidates obtain pharmaceutical approval regardless of their modalities, almost no case can escape preclinical studies on pharmacological effects using animal disease models. Plenty of medication candidates were not successful in humans although they have good effects in AD mouse models. Now there are over 200 mouse models available for AD research and these mice differ in their characteristics such as timing of Aβ plaque formation, Aβ species produced in the brain, presence of

neurodegeneration or cognitive dysfunction or tau pathology, and others. In preclinical studies, we should use disease model mice that will fit their research plans. To date, we cannot access an ultimate AD model mouse that recapitulate Aβ deposition followed by tau pathology and cognitive impairment in order in their lives, as seen in humans. We thus need to select appropriate models that have key features allowing us to precisely evaluate effects of drug candidates.

I can offer two additional choices of AD model mice by developing new *App* knock-in mice to overcome the weaknesses of the conventional models. $App^{NL\text{-}F}Psen1^{P117L}$ mice are useful for preclinical studies of Aβ metabolism and clearance including immunotherapy against wild-type Aβ. This line showed early pathological amyloidosis which is similar to observations seen in human. In addition, I also produced successfully $App^{G\text{-}F}$ knock-in mice devoid of the Swedish mutation. The $App^{G\text{-}F}$ line can be a more suitable model to study Aβ-producing secretase inhibitors. This line is the first AD mouse model that recapitulates amyloid pathology in the brain, not harboring the Swedish mutation and not depending on APP overexpression. These mice however include some hard-to-use aspects such as unknown effects derived from multiple mutations in *App* and *Psen1* genes, no tau pathology and no neurodegeneration, indicating that researchers pay careful attention to which model to use for their experimentations.

It should be noted that the most important issue has not been solved in AD drug development. The issue is the fact we do not know fundamental causes and pathomechanisms of AD, which makes it harder to develop treatment strategies. We also have to identify reliable biomarkers that can be used to monitor disease progression and therapeutic response.

I hope that the new mouse models that I developed will help fill a gap between nonclinical and clinical studies and help accelerate the development of therapeutic approaches to conquer preclinical AD in the near future.

References

1. Alzheimer, A., et al., *An English translation of Alzheimer's 1907 paper, "Uber eine eigenartige Erkankung der Hirnrinde".* Clin Anat, 1995. **8**(6): p. 429-31.
2. Maurer, K., S. Volk, and H. Gerbaldo, *Auguste D and Alzheimer's disease.* Lancet, 1997. **349**(9064): p. 1546-9.
3. Braak, H. and E. Braak, *Neuropathological stageing of Alzheimer-related changes.* Acta Neuropathol, 1991. **82**(4): p. 239-59.
4. Braak, H., et al., *Stages of the pathologic process in Alzheimer disease: age categories from 1 to 100 years.* J Neuropathol Exp Neurol, 2011. **70**(11): p. 960-9.
5. Serrano-Pozo, A., et al., *Neuropathological alterations in Alzheimer disease.* Cold Spring Harb Perspect Med, 2011. **1**(1): p. a006189.
6. Kolarova, M., et al., *Structure and pathology of tau protein in Alzheimer disease.* Int J Alzheimers Dis, 2012. **2012**: p. 731526.
7. Rasquin, S.M., J. Lodder, and F.R. Verhey, *Predictors of reversible mild cognitive impairment after stroke: a 2-year follow-up study.* J Neurol Sci, 2005. **229-230**: p. 21-5.
8. Bateman, R.J., et al., *Clinical and biomarker changes in dominantly inherited Alzheimer's disease.* N Engl J Med, 2012. **367**(9): p. 795-804.
9. Gilman, S., et al., *Clinical effects of Abeta immunization (AN1792) in patients with AD in an interrupted trial.* Neurology, 2005. **64**(9): p. 1553-62.
10. Mably, A.J., et al., *Anti-Abeta antibodies incapable of reducing cerebral Abeta oligomers fail to attenuate spatial reference memory deficits in J20 mice.* Neurobiol Dis, 2015. **82**: p. 372-384.
11. Sevigny, J., et al., *The antibody aducanumab reduces Abeta plaques in Alzheimer's disease.* Nature, 2016. **537**(7618): p. 50-6.
12. Fleck, L.M., *Alzheimer's and Aducanumab: Unjust Profits and False Hopes.* Hastings Cent Rep, 2021. **51**(4).
13. Hemingway-Eltomey, J.M. and A.J. Lerner, *Adverse effects of donepezil in treating Alzheimer's disease associated with Down's syndrome.* Am J Psychiatry, 1999. **156**(9): p. 1470.
14. Nordberg, A. and A.L. Svensson, *Cholinesterase inhibitors in the treatment of Alzheimer's disease: a comparison of tolerability and pharmacology.* Drug Saf, 1998. **19**(6): p. 465-80.
15. Jackson, S., R.J. Ham, and D. Wilkinson, *The safety and tolerability of donepezil in patients with Alzheimer's disease.* Br J Clin Pharmacol, 2004. **58 Suppl 1**: p. 1-8.
16. Breijyeh, Z. and R. Karaman, *Comprehensive Review on Alzheimer's Disease: Causes and Treatment.* Molecules, 2020. **25**(24).

17. Vemuri, P. and C.R. Jack, Jr., *Role of structural MRI in Alzheimer's disease.* Alzheimers Res Ther, 2010. **2**(4): p. 23.
18. Dawkins, E. and D.H. Small, *Insights into the physiological function of the beta-amyloid precursor protein: beyond Alzheimer's disease.* J Neurochem, 2014. **129**(5): p. 756-69.
19. Willem, M., et al., *eta-Secretase processing of APP inhibits neuronal activity in the hippocampus.* Nature, 2015. **526**(7573): p. 443-7.
20. Zheng, H., et al., *beta-Amyloid precursor protein-deficient mice show reactive gliosis and decreased locomotor activity.* Cell, 1995. **81**(4): p. 525-31.
21. Senechal, Y., P.H. Kelly, and K.K. Dev, *Amyloid precursor protein knockout mice show age-dependent deficits in passive avoidance learning.* Behav Brain Res, 2008. **186**(1): p. 126-32.
22. Koike, M.A., et al., *APP knockout mice experience acute mortality as the result of ischemia.* PLoS One, 2012. **7**(8): p. e42665.
23. Tackenberg, C. and R.M. Nitsch, *The secreted APP ectodomain sAPPalpha, but not sAPPbeta, protects neurons against Abeta oligomer-induced dendritic spine loss and increased tau phosphorylation.* Mol Brain, 2019. **12**(1): p. 27.
24. Kuester, M., et al., *The crystal structure of death receptor 6 (DR6): a potential receptor of the amyloid precursor protein (APP).* J Mol Biol, 2011. **409**(2): p. 189-201.
25. Yagishita, S., et al., *Abeta46 is processed to Abeta40 and Abeta43, but not to Abeta42, in the low density membrane domains.* J Biol Chem, 2008. **283**(2): p. 733-8.
26. Tomita, T., et al., *C terminus of presenilin is required for overproduction of amyloidogenic Abeta42 through stabilization and endoproteolysis of presenilin.* J Neurosci, 1999. **19**(24): p. 10627-34.
27. Selkoe, D.J., *Alzheimer's disease: genes, proteins, and therapy.* Physiol Rev, 2001. **81**(2): p. 741-66.
28. Kojro, E. and F. Fahrenholz, *The non-amyloidogenic pathway: structure and function of alpha-secretases.* Subcell Biochem, 2005. **38**: p. 105-27.
29. Hutton, M. and J. Hardy, *The presenilins and Alzheimer's disease.* Hum Mol Genet, 1997. **6**(10): p. 1639-46.
30. van Es, J.H., et al., *Notch/gamma-secretase inhibition turns proliferative cells in intestinal crypts and adenomas into goblet cells.* Nature, 2005. **435**(7044): p. 959-63.
31. Thinakaran, G., et al., *Endoproteolysis of presenilin 1 and accumulation of processed derivatives in vivo.* Neuron, 1996. **17**(1): p. 181-90.
32. Watanabe, H. and J. Shen, *Dominant negative mechanism of Presenilin-1 mutations in FAD.* Proc Natl Acad Sci U S A, 2017. **114**(48): p. 12635-12637.
33. Thinakaran, G., et al., *Evidence that levels of presenilins (PS1 and PS2) are coordinately*

regulated by competition for limiting cellular factors. J Biol Chem, 1997. **272**(45): p. 28415-22.

34. Shen, J., et al., *Skeletal and CNS defects in Presenilin-1-deficient mice.* Cell, 1997. **89**(4): p. 629-39.
35. Yu, H., et al., *APP processing and synaptic plasticity in presenilin-1 conditional knockout mice.* Neuron, 2001. **31**(5): p. 713-26.
36. Zhang, D.L., et al., *Oxidative damage increased in presenilin1/presenilin2 conditional double knockout mice.* Neurosci Bull, 2009. **25**(3): p. 131-7.
37. Jiang, X., et al., *Increased inflammatory response both in brain and in periphery in presenilin 1 and presenilin 2 conditional double knock-out mice.* J Alzheimers Dis, 2009. **18**(3): p. 515-23.
38. Bali, J., et al., *Role of genes linked to sporadic Alzheimer's disease risk in the production of beta-amyloid peptides.* Proc Natl Acad Sci U S A, 2012. **109**(38): p. 15307-11.
39. Rabe, S., et al., *The Swedish APP mutation alters the effect of genetically reduced BACE1 expression on the APP processing.* J Neurochem, 2011. **119**(1): p. 231-9.
40. Mullan, M., et al., *A pathogenic mutation for probable Alzheimer's disease in the APP gene at the N-terminus of beta-amyloid.* Nat Genet, 1992. **1**(5): p. 345-7.
41. Sasaguri, H., et al., *Introduction of pathogenic mutations into the mouse Psen1 gene by Base Editor and Target-AID.* Nat Commun, 2018. **9**(1): p. 2892.
42. Potter, R., et al., *Increased in vivo amyloid-beta42 production, exchange, and loss in presenilin mutation carriers.* Sci Transl Med, 2013. **5**(189): p. 189ra77.
43. Kokawa, A., et al., *The A673T mutation in the amyloid precursor protein reduces the production of beta-amyloid protein from its beta-carboxyl terminal fragment in cells.* Acta Neuropathol Commun, 2015. **3**: p. 66.
44. Maloney, J.A., et al., *Molecular mechanisms of Alzheimer disease protection by the A673T allele of amyloid precursor protein.* J Biol Chem, 2014. **289**(45): p. 30990-1000.
45. Jonsson, T., et al., *A mutation in APP protects against Alzheimer's disease and age-related cognitive decline.* Nature, 2012. **488**(7409): p. 96-9.
46. Blessed, G., B.E. Tomlinson, and M. Roth, *The association between quantitative measures of dementia and of senile change in the cerebral grey matter of elderly subjects.* Br J Psychiatry, 1968. **114**(512): p. 797-811.
47. Nagata, K., et al., *Generation of App knock-in mice reveals deletion mutations protective against Alzheimer's disease-like pathology.* Nat Commun, 2018. **9**(1): p. 1800.
48. Sasaguri, H., et al., *APP mouse models for Alzheimer's disease preclinical studies.* Embo j, 2017. **36**(17): p. 2473-2487.
49. Kwart, D., et al., *A Large Panel of Isogenic APP and PSEN1 Mutant Human iPSC*

Neurons Reveals Shared Endosomal Abnormalities Mediated by APP β-CTFs, Not Aβ. Neuron, 2019. **104**(2): p. 256-270.e5.

50. Nalivaeva, N.N., et al., *Amyloid-clearing proteins and their epigenetic regulation as a therapeutic target in Alzheimer's disease.* Front Aging Neurosci, 2014. **6**: p. 235.
51. Saito, T., et al., *Calpain Activation in Alzheimer's Model Mice Is an Artifact of APP and Presenilin Overexpression.* J Neurosci, 2016. **36**(38): p. 9933-6.
52. Higuchi, M., et al., *Mechanistic involvement of the calpain-calpastatin system in Alzheimer neuropathology.* Faseb j, 2012. **26**(3): p. 1204-17.
53. Hashimoto, S., et al., *Endoplasmic reticulum stress responses in mouse models of Alzheimer's disease: Overexpression paradigm versus knockin paradigm.* J Biol Chem, 2018. **293**(9): p. 3118-3125.
54. Gamache, J., et al., *Factors other than hTau overexpression that contribute to tauopathy-like phenotype in rTg4510 mice.* Nat Commun, 2019. **10**(1): p. 2479.
55. Citron, M., et al., *Mutation of the beta-amyloid precursor protein in familial Alzheimer's disease increases beta-protein production.* Nature, 1992. **360**(6405): p. 672-4.
56. Lichtenthaler, S.F., et al., *Mechanism of the cleavage specificity of Alzheimer's disease gamma-secretase identified by phenylalanine-scanning mutagenesis of the transmembrane domain of the amyloid precursor protein.* Proc Natl Acad Sci U S A, 1999. **96**(6): p. 3053-8.
57. Nilsberth, C., et al., *The 'Arctic' APP mutation (E693G) causes Alzheimer's disease by enhanced Abeta protofibril formation.* Nat Neurosci, 2001. **4**(9): p. 887-93.
58. Saito, T., et al., *Single App knock-in mouse models of Alzheimer's disease.* Nat Neurosci, 2014. **17**(5): p. 661-3.
59. Masuda, A., et al., *Cognitive deficits in single App knock-in mouse models.* Neurobiol Learn Mem, 2016. **135**: p. 73-82.
60. Christian, M., et al., *Targeting DNA double-strand breaks with TAL effector nucleases.* Genetics, 2010. **186**(2): p. 757-61.
61. Kim, Y.G., J. Cha, and S. Chandrasegaran, *Hybrid restriction enzymes: zinc finger fusions to Fok I cleavage domain.* Proc Natl Acad Sci U S A, 1996. **93**(3): p. 1156-60.
62. Ran, F.A., et al., *Genome engineering using the CRISPR-Cas9 system.* Nat Protoc, 2013. **8**(11): p. 2281-2308.
63. Jinek, M., et al., *A programmable dual-RNA-guided DNA endonuclease in adaptive bacterial immunity.* Science, 2012. **337**(6096): p. 816-21.
64. Ran, F.A., et al., *In vivo genome editing using Staphylococcus aureus Cas9.* Nature, 2015. **520**(7546): p. 186-91.
65. Nishimasu, H., et al., *Crystal Structure of Staphylococcus aureus Cas9.* Cell, 2015. **162**(5):

p. 1113-26.

66. Lee, J.K., et al., *Directed evolution of CRISPR-Cas9 to increase its specificity.* Nat Commun, 2018. **9**(1): p. 3048.

67. Hu, J.H., et al., *Evolved Cas9 variants with broad PAM compatibility and high DNA specificity.* Nature, 2018. **556**(7699): p. 57-63.

68. Komor, A.C., et al., *Programmable editing of a target base in genomic DNA without double-stranded DNA cleavage.* Nature, 2016. **533**(7603): p. 420-4.

69. Porto, E.M., et al., *Base editing: advances and therapeutic opportunities.* Nat Rev Drug Discov, 2020. **19**(12): p. 839-859.

70. Cataldo, A.M., et al., *Endocytic pathway abnormalities precede amyloid beta deposition in sporadic Alzheimer's disease and Down syndrome: differential effects of APOE genotype and presenilin mutations.* Am J Pathol, 2000. **157**(1): p. 277-86.

71. Nixon, R.A., *Endosome function and dysfunction in Alzheimer's disease and other neurodegenerative diseases.* Neurobiol Aging, 2005. **26**(3): p. 373-82.

72. Karch, C.M. and A.M. Goate, *Alzheimer's disease risk genes and mechanisms of disease pathogenesis.* Biol Psychiatry, 2015. **77**(1): p. 43-51.

73. Lauritzen, I., et al., *Intraneuronal aggregation of the β-CTF fragment of APP (C99) induces Aβ-independent lysosomal-autophagic pathology.* Acta Neuropathol, 2016. **132**(2): p. 257-276.

74. Hsu, P.D., et al., *DNA targeting specificity of RNA-guided Cas9 nucleases.* Nat Biotechnol, 2013. **31**(9): p. 827-32.

75. Yang, H., H. Wang, and R. Jaenisch, *Generating genetically modified mice using CRISPR/Cas-mediated genome engineering.* Nat Protoc, 2014. **9**(8): p. 1956-68.

76. Cradick, T.J., et al., *COSMID: A Web-based Tool for Identifying and Validating CRISPR/Cas Off-target Sites.* Mol Ther Nucleic Acids, 2014. **3**: p. e214.

77. Bae, S., J. Park, and J.S. Kim, *Cas-OFFinder: a fast and versatile algorithm that searches for potential off-target sites of Cas9 RNA-guided endonucleases.* Bioinformatics, 2014. **30**(10): p. 1473-5.

78. Enya, M., et al., *Appearance of sodium dodecyl sulfate-stable amyloid beta-protein (Abeta) dimer in the cortex during aging.* Am J Pathol, 1999. **154**(1): p. 271-9.

79. Saido, T.C., et al., *Dominant and differential deposition of distinct beta-amyloid peptide species, A beta N3(pE), in senile plaques.* Neuron, 1995. **14**(2): p. 457-66.

80. Saido, T.C., et al., *Spatial resolution of the primary beta-amyloidogenic process induced in postischemic hippocampus.* J Biol Chem, 1994. **269**(21): p. 15253-7.

81. Kennedy, M.E., et al., *The BACE1 inhibitor verubecestat (MK-8931) reduces CNS beta-amyloid in animal models and in Alzheimer's disease patients.* Sci Transl Med, 2016.

8(363): p. 363ra150.

82. Saito, T., et al., *Potent amyloidogenicity and pathogenicity of Abeta43.* Nat Neurosci, 2011. **14**(8): p. 1023-32.
83. Saido, T.C. and N. Iwata, *Metabolism of amyloid beta peptide and pathogenesis of Alzheimer's disease. Towards presymptomatic diagnosis, prevention and therapy.* Neurosci Res, 2006. **54**(4): p. 235-53.
84. Shimojo, M., et al., *Enzymatic characteristics of I213T mutant presenilin-1/gamma-secretase in cell models and knock-in mouse brains: familial Alzheimer disease-linked mutation impairs gamma-site cleavage of amyloid precursor protein C-terminal fragment beta.* J Biol Chem, 2008. **283**(24): p. 16488-96.
85. Qi-Takahara, Y., et al., *Longer forms of amyloid beta protein: implications for the mechanism of intramembrane cleavage by gamma-secretase.* J Neurosci, 2005. **25**(2): p. 436-45.
86. Takami, M., et al., *gamma-Secretase: successive tripeptide and tetrapeptide release from the transmembrane domain of beta-carboxyl terminal fragment.* J Neurosci, 2009. **29**(41): p. 13042-52.
87. Thal, D.R., et al., *Phases of A beta-deposition in the human brain and its relevance for the development of AD.* Neurology, 2002. **58**(12): p. 1791-800.
88. Boon, B.D.C., et al., *The coarse-grained plaque: a divergent Abeta plaque-type in early-onset Alzheimer's disease.* Acta Neuropathol, 2020. **140**(6): p. 811-830.
89. Fukumoto, H., et al., *Amyloid beta protein deposition in normal aging has the same characteristics as that in Alzheimer's disease. Predominance of A beta 42(43) and association of A beta 40 with cored plaques.* Am J Pathol, 1996. **148**(1): p. 259-65.
90. Iwatsubo, T., et al., *Visualization of A beta 42(43) and A beta 40 in senile plaques with end-specific A beta monoclonals: evidence that an initially deposited species is A beta 42(43).* Neuron, 1994. **13**(1): p. 45-53.
91. Sato, K., et al., *Fluoro-substituted and 13C-labeled styrylbenzene derivatives for detecting brain amyloid plaques.* Eur J Med Chem, 2004. **39**(7): p. 573-8.
92. Higuchi, M., et al., *19F and 1H MRI detection of amyloid beta plaques in vivo.* Nat Neurosci, 2005. **8**(4): p. 527-33.
93. Heneka, M.T., et al., *Neuroinflammation in Alzheimer's disease.* Lancet Neurol, 2015. **14**(4): p. 388-405.
94. Nicoll, J.A., et al., *Neuropathology of human Alzheimer disease after immunization with amyloid-beta peptide: a case report.* Nat Med, 2003. **9**(4): p. 448-52.
95. Lewcock, J.W., et al., *Emerging Microglia Biology Defines Novel Therapeutic Approaches for Alzheimer's Disease.* Neuron, 2020. **108**(5): p. 801-821.

96. Podlesny-Drabiniok, A., E. Marcora, and A.M. Goate, *Microglial Phagocytosis: A Disease-Associated Process Emerging from Alzheimer's Disease Genetics.* Trends Neurosci, 2020. **43**(12): p. 965-979.

97. Qin, Q., et al., *TREM2, microglia, and Alzheimer's disease.* Mech Ageing Dev, 2021. **195**: p. 111438.

98. Yamakawa, H., et al., *beta-Secretase inhibitor potency is decreased by aberrant beta-cleavage location of the "Swedish mutant" amyloid precursor protein.* J Biol Chem, 2010. **285**(3): p. 1634-42.

99. Hussain, I., et al., *Oral administration of a potent and selective non-peptidic BACE-1 inhibitor decreases beta-cleavage of amyloid precursor protein and amyloid-beta production in vivo.* J Neurochem, 2007. **100**(3): p. 802-9.

100. Li, S., et al., *Swedish mutant APP-based BACE1 binding site peptide reduces APP β-cleavage and cerebral Aβ levels in Alzheimer's mice.* Sci Rep, 2015. **5**: p. 11322.

101. Tsubuki, S., Y. Takaki, and T.C. Saido, *Dutch, Flemish, Italian, and Arctic mutations of APP and resistance of Abeta to physiologically relevant proteolytic degradation.* Lancet, 2003. **361**(9373): p. 1957-8.

102. Ruiz-Riquelme, A., et al., *Aβ43 aggregates exhibit enhanced prion-like seeding activity in mice.* Acta Neuropathol Commun, 2021. **9**(1): p. 83.

103. Flood, D.G., et al., *FAD mutant PS-1 gene-targeted mice: increased A beta 42 and A beta deposition without APP overproduction.* Neurobiol Aging, 2002. **23**(3): p. 335-48.

104. Li, H., et al., *Vascular and parenchymal amyloid pathology in an Alzheimer disease knock-in mouse model: interplay with cerebral blood flow.* Mol Neurodegener, 2014. **9**: p. 28.

105. Saito, T., et al., *Somatostatin regulates brain amyloid beta peptide Abeta42 through modulation of proteolytic degradation.* Nat Med, 2005. **11**(4): p. 434-9.

106. Kalimo, H., et al., *The Arctic AbetaPP mutation leads to Alzheimer's disease pathology with highly variable topographic deposition of differentially truncated Abeta.* Acta Neuropathol Commun, 2013. **1**: p. 60.

107. Hung, C.O.Y. and F.J. Livesey, *Altered γ-Secretase Processing of APP Disrupts Lysosome and Autophagosome Function in Monogenic Alzheimer's Disease.* Cell Rep, 2018. **25**(13): p. 3647-3660.e2.

108. Jiang, Y., et al., *Alzheimer's-related endosome dysfunction in Down syndrome is Abeta-independent but requires APP and is reversed by BACE-1 inhibition.* Proc Natl Acad Sci U S A, 2010. **107**(4): p. 1630-5.

109. Kim, S., et al., *Evidence that the rab5 effector APPL1 mediates APP-βCTF-induced dysfunction of endosomes in Down syndrome and Alzheimer's disease.* Mol Psychiatry, 2016. **21**(5): p. 707-16.

110. Woodruff, G., et al., *Defective Transcytosis of APP and Lipoproteins in Human iPSC-Derived Neurons with Familial Alzheimer's Disease Mutations.* Cell Rep, 2016. **17**(3): p. 759-773.
111. Xu, W., et al., *Amyloid precursor protein-mediated endocytic pathway disruption induces axonal dysfunction and neurodegeneration.* J Clin Invest, 2016. **126**(5): p. 1815-33.
112. Treusch, S., et al., *Functional links between Aβ toxicity, endocytic trafficking, and Alzheimer's disease risk factors in yeast.* Science, 2011. **334**(6060): p. 1241-5.
113. Willen, K., et al., *Abeta accumulation causes MVB enlargement and is modelled by dominant negative VPS4A.* Mol Neurodegener, 2017. **12**(1): p. 61.
114. Marshall, K.E., et al., *Misfolded amyloid-β-42 impairs the endosomal-lysosomal pathway.* Cell Mol Life Sci, 2020.
115. Baglietto-Vargas, D., et al., *Generation of a humanized Abeta expressing mouse demonstrating aspects of Alzheimer's disease-like pathology.* Nat Commun, 2021. **12**(1): p. 2421.
116. Knupp, A., et al., *Depletion of the AD Risk Gene SORL1 Selectively Impairs Neuronal Endosomal Traffic Independent of Amyloidogenic APP Processing.* Cell Rep, 2020. **31**(9): p. 107719.
117. Pensalfini, A., et al., *Endosomal Dysfunction Induced by Directly Overactivating Rab5 Recapitulates Prodromal and Neurodegenerative Features of Alzheimer's Disease.* Cell Rep, 2020. **33**(8): p. 108420.
118. Elvang, A.B., et al., *Differential effects of gamma-secretase and BACE1 inhibition on brain Abeta levels in vitro and in vivo.* J Neurochem, 2009. **110**(5): p. 1377-87.
119. Cummings, J.L., T. Morstorf, and K. Zhong, *Alzheimer's disease drug-development pipeline: few candidates, frequent failures.* Alzheimers Res Ther, 2014. **6**(4): p. 37.

Supplemental Figure 1

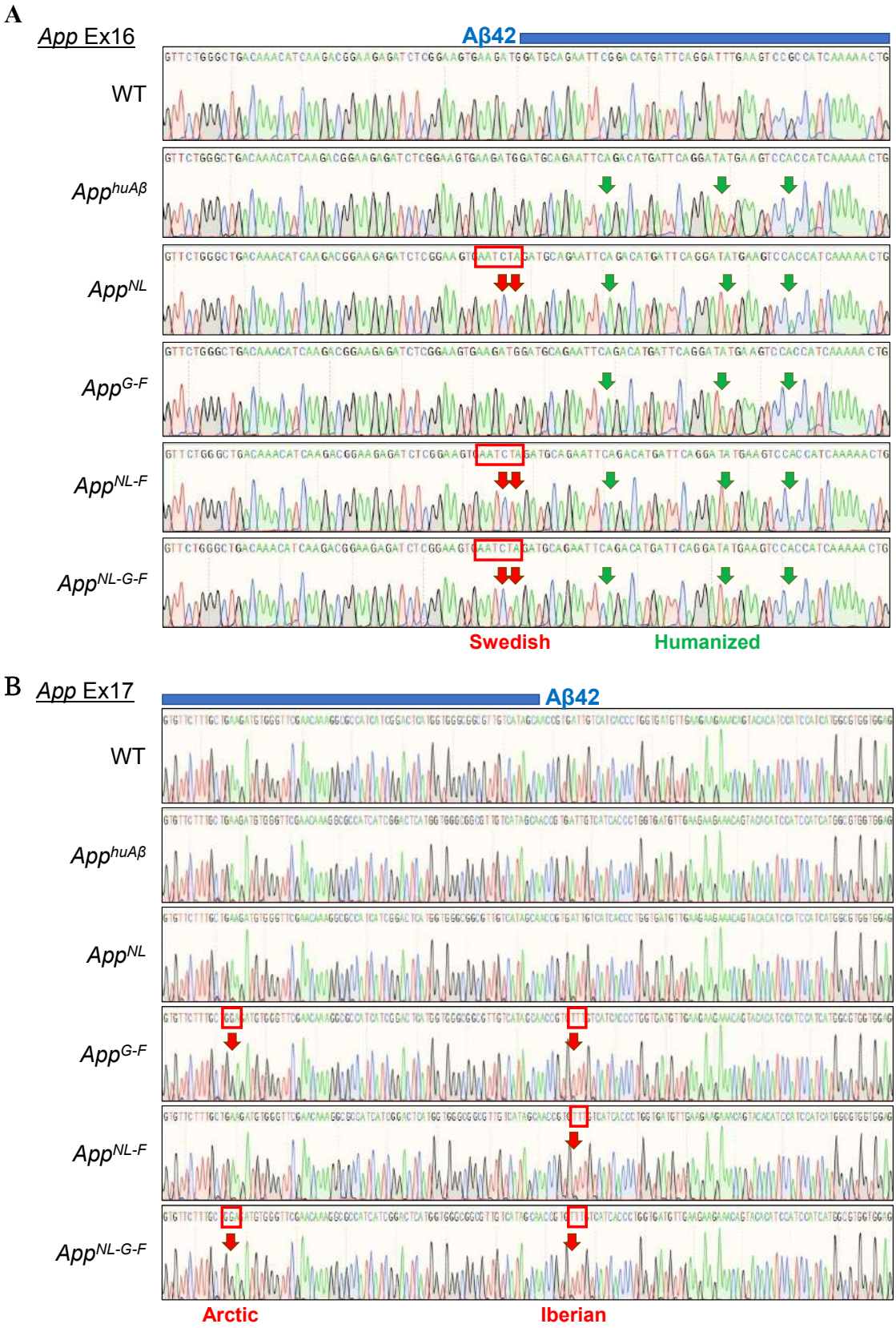

C

Fig. S1. Exon sequences of the *App* gene in *App* knock-in mouse lines encoding CTF-β.

Sequencing analyses of *App* exon 16 (A), exon 17 (B) and exon 18 (C) indicate that all genotypes of the *App* knock-in mice share identical amino acid sequences except for the artificially introduced mutations. These data indicate that the difference in the electrophoretic mobility of CTF-β between each line shown in **Fig. 14A** can be solely attributed to the intentionally altered mutations introduced.

Supplemental Figure 2

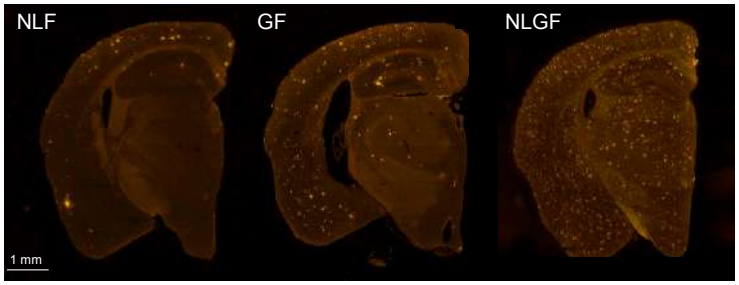

Fig. S2. Aβ plaque formation in the brains of 12-month-old *App*$^{NL-F}$, *App*$^{G-F}$ and *App*$^{NL-G-F}$ mice.

Immunohistochemistry images with N1D antibody detection show that *App*$^{G-F}$ mice exhibited more and less prominent amyloid pathology than *App*$^{NL-F}$ and *App*$^{NL-G-F}$ mice, respectively, at 12 months.

Supplemental Figure 3

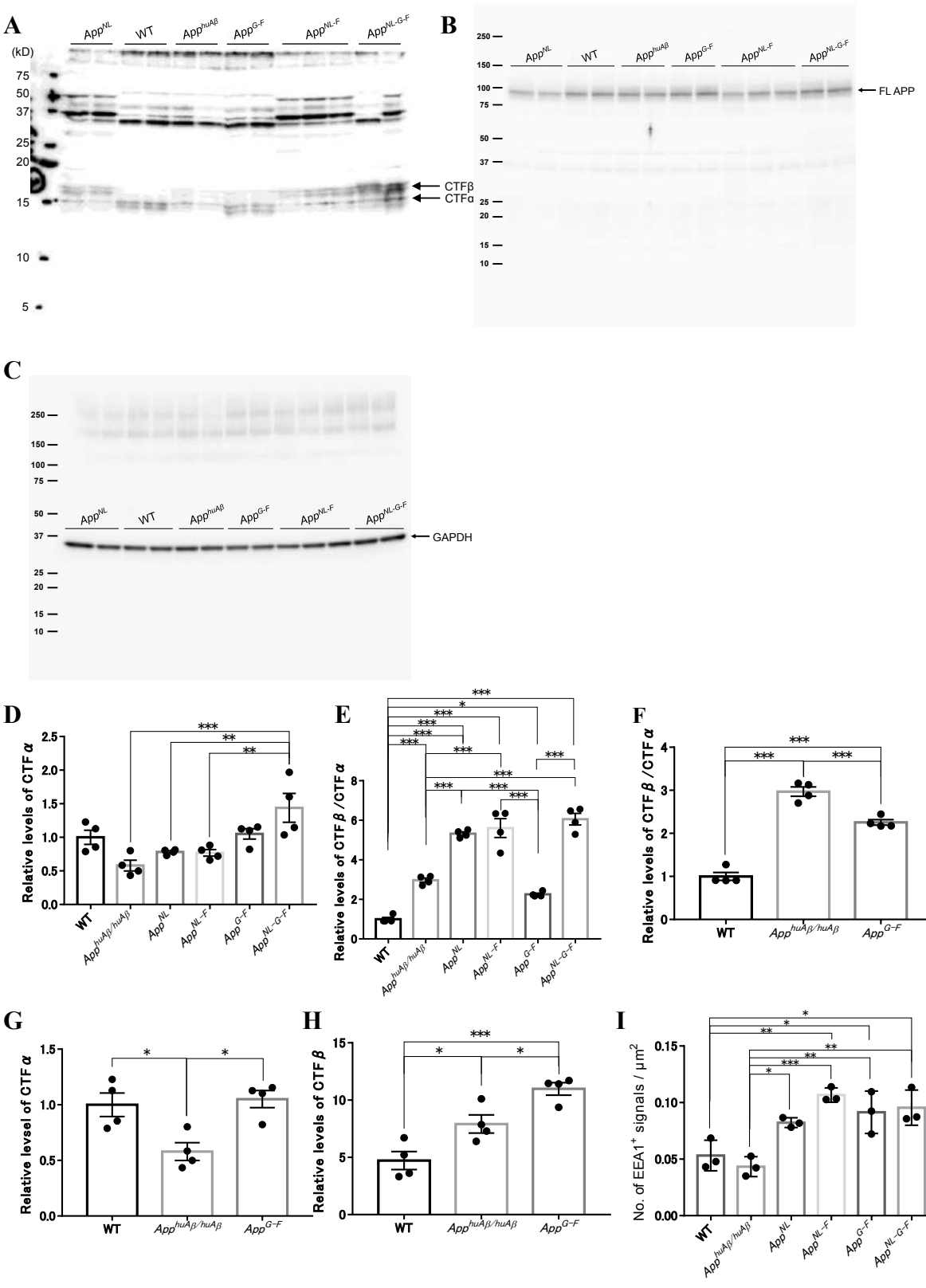

Fig. S3. Analysis of APP CTFs and endosomal abnormalities.

(A-C) Full-blots of APP CTFs (A) and full-length APP (B) and GAPDH (C) using the cortices of 12-month-old *App* knock-in lines used in **Fig. 4** are shown. (D) Intensities of CTF-α-immunoreactive bands were quantified and statistically analyzed for WT, $App^{huA\beta}$, App^{NL}, $App^{NL\text{-}F}$, $App^{G\text{-}F}$ and $App^{NL\text{-}G\text{-}F}$ mice. (E) Relative levels of CTF-β/CTF-α ratio compared to WT mice. (E-G) Relative levels of CTF-α (F), CTF-β (G) and CTF-β/CTF-α ratios (H) were statistically analysed for WT, $App^{huA\beta}$ and $App^{G\text{-}F}$ mice. Each bar represents the mean ± SEM. * $P < 0.05$, ** $P < 0.01$, *** $P < 0.001$. WT, $App^{huA\beta}$, App^{NL}, $App^{NL\text{-}F}$, $App^{G\text{-}F}$ and $App^{NL\text{-}G\text{-}F}$; n=4 for each genotype. (I) Number of $EEA1^{+}$ signals per μm^2 was increased in *App* knock-in mice except for $App^{huA\beta}$ mice. WT, $App^{huA\beta}$, App^{NL}, $App^{NL\text{-}F}$, $App^{G\text{-}F}$ and $App^{NL\text{-}G\text{-}F}$; n=3 for each genotype, one-way ANOVA followed by Turkey's multiple comparison test.

Supplementary Figure 4

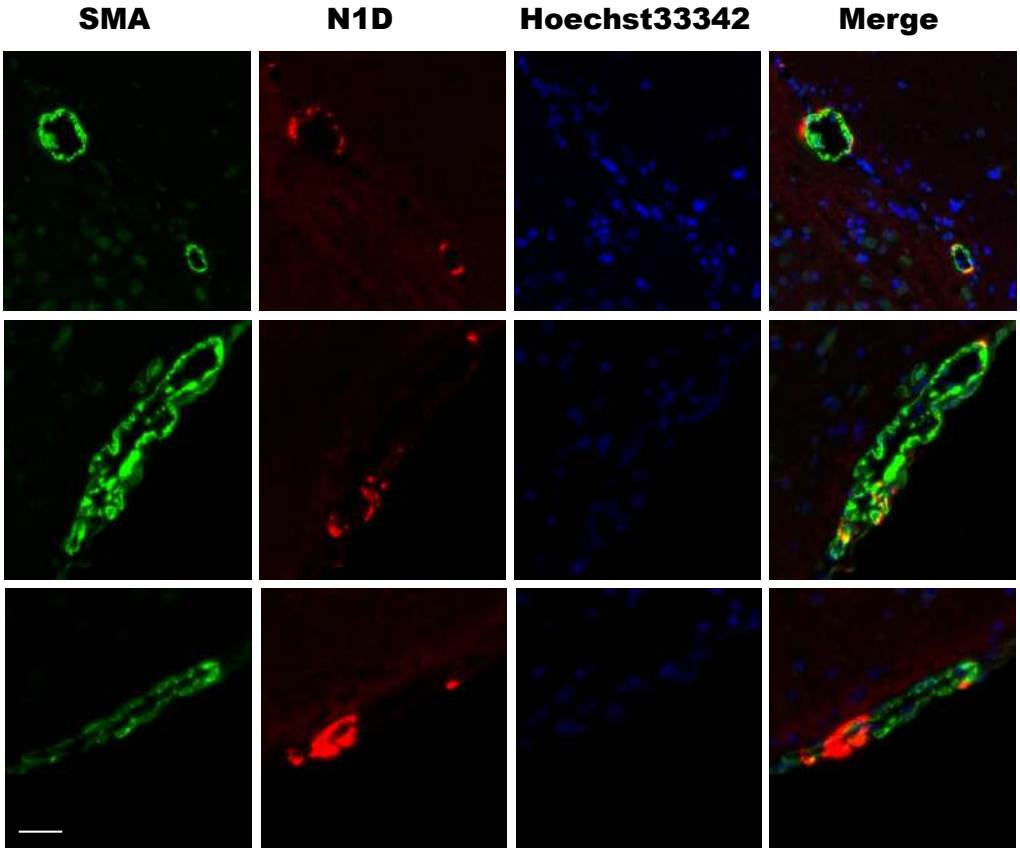

Fig. S4. CAA-like pathology in *AppPsen1* double mutant mice

Representative images of CAA in the meningeal blood vessels of 12-month-old $App^{NL-F}\times Psen1^{P117L}$ mice. SMA (smooth muscle actin) marks blood vessels (green). N1D represents Aβ deposition (red). Hoechst33342 binds to dsDNA (blue). The Scale bar indicates 25 μm.

Acknowledgements

First and foremost, I would like to sincerely express my appreciation to my supervisor Professor Toshio Ohshima for all that he has done to help me since I enrolled in Graduate School of Advanced Science and Engineering, Waseda University. I could not have spent my 5-year life as a graduate student without his continuous support.

I would like to deeply thank Dr, Takaomi Saido in RIKEN CBS for all his support. I cannot find the words to thank him enough for welcoming my sudden visit in 2017. His thoughtful comments always guided me to the right path to accomplish my research works. I am also grateful to Dr. Hiroki Sasaguri in RIKEN CBS and Kenichi Nagata in Nagoya University and Professor Takafumi Inoue for their valuable advices and suggestions.

I would like to express deepest gratitude to members from Ohshima laboratory, Saido laboratory and Inoue laboratory for kindly supporting my daily life.

Finally, I wish to offer my profound gratitude to my family. I will pay back a belated dept of gratitude to them.

Research achievements

Publications

1. **Kaori Sato**[*], Naoto Watamura[*], Ryo Fujioka, Naomi Mihira, Misaki Sekiguchi, Kenichi Nagata, Toshio Ohshima, Takashi Saito, Takaomi C. Saido and Hiroki Sasaguri. A 3rd generation mouse model of Alzheimer's disease shows early and increased cored plaque pathology composed of wild-type human amyloid β peptide. *J Biol Chem*. (2021) 101004. *These authors contributed equally to this work.

2. Naoto Watamura[*], **Kaori Sato**[*], Gen Shiihashi, Ayami Iwasaki, Naoko Kamano, Mika Takahashi, Misaki Sekiguchi, Naomi Yamazaki, Ryo Fujioka, Kenichi Nagata, Takashi Saito, Toshio Ohshima, Takaomi C. Saido and Hiroki Sasaguri. An isogenic panel of single *App* knock-in mouse models of Alzheimer's disease confers differential profiles of β-secretase inhibition and endosomal abnormalities. *These authors contributed equally to this work. *bioRxiv*, doi: https://doi.org/10.1101/2021.08.22.457278

3. Kenichi Nagata, Mika Takahashi, Yukio Matsuba, Fumi Okuyama-Uchimura, **Kaori Sato**, Shoko Hashimoto, Takashi Saito and Takaomi C. Saido. Generation of App knock-in mice reveals deletion mutations protective against Alzheimer's disease-like pathology. *Nature Communications*, 9(1):1800 (2018)

4. Hiroki Sasaguri, Kenichi Nagata, Misaki Sekiguchi, Ryo Fujioka, Yukio Matsuba,

Shoko Hashimoto, **Kaori Sato**, Deepika Kurup, Takanori Yokota and Takaomi C. Saido. Introduction of pathogenic mutations into the mouse Psen1 gene by Base Editor and Target-AID. *Nature Communications*, 9(1):2892 (2018)

Presentations

1. **Kaori Sato**. Recent advancement in modeling Alzheimer's disease. The CBS Young Investigators' Seminar and Social, Saitama, Japan, 2021.6 (oral)

2. **Kaori Sato**, Kenichi Nagata, Takaomi Saido, Hiroki Sasaguri. The combined effects of pathogenic mutations in the *App* and *Psen1* genes *in vivo*. The 39th annual meeting of Japan society for dementia research. Aichi, Japan (changed to hybrid conference due to COVID-19 pandemic), 2020.11 (poster)

3. **Kaori Sato**, Kenichi Nagata, Takaomi Saido, Hiroki Sasaguri. The effects of pathogenic mutations in the *App* and *Psen1* genes on *in vivo* γ-secretase activity are additive. Alzheimer's association international conference 2020, Amsterdam, Netherland (unfortunately changed to virtual conference due to COVID-19 pandemic), 2020.7 (poster)

4. **Kaori Sato**, Kenichi Nagata, Hiroki Sasaguri, Toshio Oshima, Takaomi Saido. 内在性プレセニリン 1 エクソン 9 欠損マウスの作製と機能解析. The 38th annual meeting of Japan society for dementia research. Tokyo, Japan, 2019.11 (poster)

5. **Kaori Sato**, Kenichi Nagata, Hiroki Sasaguri, Toshio Oshima, Takaomi Saido. Introduction of deletion mutation associated with Alzheimer's disease into mouse genome. Neuroscience 2019, Chicago, America, 2019.10 (poster)

6. **Kaori Sato**, Kenichi Nagata, Hiroki Sasaguri, Toshio Oshima, Takaomi Saido. Introduction of deletion mutation associated with Alzheimer's disease into mouse genome. The international fellows poster session at neuroscience 2019. Chicago, America, 2019.10 (poster)

7. **Kaori Sato**, Kenichi Nagata, Hiroki Sasaguri, Toshio Oshima, Takaomi Saido. CRISPR/Cas-mediated generation of *Presenilin1* mutant mouse models with Alzheimer's disease associated mutations. The 71st annual scientific meeting of the American association for clinical chemistry. Anaheim, America, 2019.8 (poster)

8. **Kaori Sato**, Kenichi Nagata, Hiroki Sasaguri, Toshio Oshima, Takaomi Saido. CRISPR/Cas-mediated generation of *Presenilin1* mutant mouse models with Alzheimer's disease associated mutations. The 2019 AACC student poster conference. Anaheim, America, 2019.8 (poster)

9. **Kaori Sato**, Hiroki Sasaguri, Kenichi Nagata, Takaomi Saido. Introduction of deletion mutations associated with Alzheimer's disease into mouse genome. 2019 年度革新脳後期キックオフシンポジウム. Kanagawa, Japan, 2019.7 (poster)

10. **Kaori Sato**, Kenichi Nagata, Hiroki Sasaguri, Toshio Oshima, Takaomi Saido. CRISPR/Cas-mediated generation of *Presenilin1* mutant mouse models with Alzheimer's disease associated mutations. The 2019 Joint Annual Meeting of the Japan Neuroscience Society and the Japanese Society for Neurochemistry. Niigata, Japan, 2019.7 (poster)

11. **Kaori Sato**, Kenichi Nagata, Hiroki Sasaguri, Toshio Oshima, Takaomi Saido. Targeted genomic deletion associated with Alzheimer's disease in mouse. The 4th annual meeting of Japan society for genome editing. Tokyo, Japan, 2019.6 (poster)

12. **Kaori Sato**, Kenichi Nagata, Hiroki Sasaguri, Toshio Oshima, Takaomi Saido. ゲノム編集技術による*Psen1*変異ノックインモデルの作製. The 37th annual meeting of Japan society for dementia research. Hokkaido, Japan. 2018.10 (poster)

13. **Kaori Sato**. ゲノム編集技術によるPsen1変異ノックインモデルの作製. 第8回認知症研究を知る若手研究者の集まり2018. Shiga, Japan. 2018.7 (oral)

14. **Kaori Sato**, Kenichi Nagata, Hiroki Sasaguri, Toshio Ohshima, Takaomi Saido. A mutant cell line of Alzheimer's disease-associated Presnilin-1 mutation using CRISPR-Cas system. The 4th annual meeting of Japan society for genome editing. Hiroshima, Japan, 2018.6 (poster)